Dictyostelium Mutants Lacking Multiple Classic Myosin I Isoforms Reveal Combinations of Shared and Distinct Functions

Goeh Jung, Xufeng Wu, and John A. Hammer III

Laboratory of Cell Biology, Section on Molecular Cell Biology, National Heart, Lung, and Blood Institute, National Institutes of Health, Bethesda, Maryland 20892-0301

Abstract. *Dictyostelium* cells that lack the myoB isoform were previously shown to exhibit reduced efficiencies of phagocytosis and chemotactic aggregation ("streaming") and to crawl at about half the speed of wild-type cells. Of the four other *Dictyostelium* myosin I isoforms identified to date, myoC and myoD are the most similar to myoB in terms of tail domain sequence. Furthermore, we show here that myoC, like myoB and myoD, is concentrated in actin-rich cortical regions like the leading edge of migrating cells. To look for evidence of functional overlap between these isoforms, we analyzed myoB, myoC, and myoD single mutants, myoB/myoD double mutants, and myoB/myoC/myoD triple mutants, which were created using a combination of gene targeting techniques and constitutive expression of antisense RNA. With regard to the speed of locomoting, aggregation-stage cells, of the three single mutants, only the myoB mutant was significantly slower. Moreover, double and triple mutants were only slightly slower than the myoB single mutant. Consistent with this, the protein level of myoB alone rises dramatically during early development, suggesting that a special demand is placed on this one isoform when cells become highly motile. We also found, however, that the absolute amount of myoB protein in aggregation-stage cells is much higher than that for myoC and myoD, suggesting that what appears to be a case of nonoverlapping function could be the result of large differences in the amounts of functionally overlapping isoforms. Streaming assays also suggest that myoC plays a significant role in some aspect of motility other than cell speed. With regard to phagocytosis, both myoB and myoC single mutants exhibited significant reductions in initial rate, suggesting that these two isoforms perform nonredundant roles in supporting the phagocytic process. In triple mutants these defects were not additive, however. Finally, because double and triple mutants exhibited significant and progressive decreases in doubling times, we also measured the kinetics of fluid phase endocytic flux (uptake, transit time, efflux). Not only do all three isoforms contribute to this process, but their contributions are synergistic. While these results, when taken together, refute the simple notion that these three "classic" myosin I isoforms perform exclusively identical functions, they do reveal that all three share in supporting at least one cellular process (endocytosis), and they identify several other processes (motility, streaming, and phagocytosis) that are supported to a significant extent by either individual isoforms or various combinations of them.

To date, 11 classes of myosin have been identified (13, 38, 47), 10 of which are considered to be unconventional (for review see 12 and 28). While all of these unconventional myosins contain the ~80-kD motor domain that corresponds in sequence to subfragment 1, their nonmotor domain sequences are widely divergent. These unique sequences are thought to confer functional specificity on a more or less generic motor domain by mediating specific interations with different cellular proteins, structures, or membranes. Central to this theme, therefore, is the idea that the variations in nonmotor domain sequences that are seen not only between members of different classes, but between different isoforms within the same class as well, signify functional specialization.

Our recent efforts have been focused on attempting to define the functions of myosins I in the cellular slime mold *Dictyostelium discoideum*. In protozoa, these single-headed, nonfilamentous, actin-based mechanoenzymes have been proposed to play important roles in pseudopod and lamellopod extension, cell migration, particle ingestion, intracellular vesicle transport, and contractile vacuole function (3, 9, 10, 18, 23, 36, 55, 61). To date, five myosin I heavy

Address all correspondence to John A. Hammer III, Laboratory of Cell Biology, Building 3, Room B1-22, National Institutes of Health, Bethesda, MD 20892-0301. Tel.: (301) 496-8960. Fax: (301) 402-1519.

chain genes have been cloned from *Dictyostelium* and fully sequenced: *myoA* (54), *myoB* (20), *myoC* (34), *myoD* (21), and *myoE* (57). While the application of gene targeting and antisense RNA techniques in these haploid amoebae represents a reasonable approach to sorting out function in vivo (8), the identification of myosin I–dependent functions will be complicated by the large number of expressed isoforms, especially if some of them have overlapping functions.

The five sequenced *Dictyostelium* myosin I isoforms can be divided into two subclasses based on their tail domain sequences. MyoB, myoC, and myoD, which collectively are referred to as "classic" myosins I, contain all three tail homology (TH)[1] regions (TH·1, TH·2, and TH·3) identified previously in the *Acanthamoeba* myosins I (12, 23, 28, 36). In the amoeba proteins, the NH_2-terminal, ~220-residue, polybasic TH·1 domain contains a binding site for anionic phospholipid membranes, while all or some portion of the central, ~185-residue, glycine-, proline-, and alanine/glutamine-rich TH·2 domain and the COOH-terminal, ~50-residue, SH3-like, TH·3 domain contains an ATP-insensitive actin-binding site (12, 23, 28, 36). Consistent with this, fusion proteins that contain portions of the tail domains of *Dictyostelium* myoB (42) and myoC (19) bind tightly to F-actin (±ATP), and this binding site resides totally within the glycine-, proline-, alanine/glutamine-rich TH·2 domain. Furthermore, like the purified *Acanthamoeba* proteins, *Dictyostelium* myoB and myoD demonstrate triphasic kinetics of actin-activation (26) and cross-link actin filaments (Lynch, T.J., H. Brzeska, and E.D. Korn. 1990. *Biophys. J.* 57:536a). Both of these properties are consistent with the existence of two actin-binding sites within a single myosin I molecule.

In contrast to myoB/myoC/myoD, *Dictyostelium* myoA and myoE possess truncated heavy chains whose tail domains end shortly after a polybasic, TH·1-like domain. Therefore, neither possesses the actin-binding site that resides within TH·2 or the SH3-like TH·3 domain, which in the classic myosins I may be involved in myosin targeting and/or signal transduction (19, 50). This striking difference in tail domain structure between the three classic and two truncated isoforms suggests that these two apparent subfamilies may support different functions in the cell. Furthermore, the strong similarities in tail domain structure between the isoforms within each apparent subfamily suggest that if functional overlaps exist, they would most likely be between isoforms within each subfamily.

Immunofluorescence localizations have revealed that myoB is concentrated within a number of actin-rich cortical domains, including pseudopods and lamellopods at the leading edge of migrating cells, sites of particle ingestion (phagocytic cups), sites of cell–cell contact, and filopodia (10; Morita, Y.S., G. Jung, J.A. Hammer III, and Y. Fukui, manuscript submitted for publication). These localizations are especially interesting since this isoform can cross-link actin filaments, and structurally similar myosins from *Acanthamoeba* have been shown not only to cross-link actin, but to generate a contractile tension within the cross-linked actin gel (3, 23, 28, 36). Therefore, these classic myosins I could serve, by virtue of their cross-linking activity, to regulate the elastic modulus of the dense isotropic actin meshworks that comprise the motile regions of these cells (17, 35, 43). Furthermore, by virtue of their regulated mechanochemical activity (12, 23, 28, 36), these isoforms should be capable of exerting a collapsing force within these regions. The effect that these myosin I–dependent activities have on the overall dynamics of cortical actin networks could allow these classic myosins I to regulate and/or power a wide range of motile processes that are dependent on cortical actin, such as the extension/retraction of pseudopods, cell migration, and phagocytosis.

Cells in which the myoB heavy chain gene has been rendered nonfunctional by a double-crossover gene replacement event exhibit abnormalities in exactly the types of motility described above (18, 61). Specifically, myoB$^-$ cells exhibit a reduced efficiency of chemotactic aggregation, locomote at 51% of the rate of wild-type cells, and exhibit an ~32% reduction in the initial rate of uptake of bacteria by phagocytosis. While these defects are quantifiable (and, therefore, not subtle), they are generally thought of as being fairly small in magnitude. One of a number of possible explanations for this is that other, closely related isoforms mitigate to some extent the defects caused by the loss of myoB through functional compensation. Of the *Dictyostelium* myosin I isoforms characterized to date, myoC and myoD would appear to be the best candidates, not only because of their structural (and biochemical) similarities, but the similarities in their intracellular localizations as well. Specifically, myoD (21) and myoC (see below), like myoB, concentrate within pseudopods at the leading edge of migrating cells. To the extent that these three classic myosin I isoforms do in fact share in supporting any particular cellular process, individual cell lines in which two or more isoforms are missing may well exhibit defects in this process that are at least additive if not synergistic.

To investigate the possibility of functional overlap between myoB, myoC, and myoD, we have characterized here myoB$^-$, myoC$^-$, and myoD$^-$ single mutants, double mutants in which myoD protein levels have been greatly reduced via antisense RNA expression in a myoB$^-$ background, and triple mutants in which myoC levels have been greatly reduced via antisense RNA expression in a double mutant background. Like the myoB$^-$ cells described previously (18, 61), all of these mutants were characterized with regard to whole cell motility, streaming behavior, and phagocytic rate. Because the double and triple mutants exhibited significant and progressive reductions in doubling times, we also characterized all these mutants with regard to the kinetics of fluid phase endocytic flux. We also determined the intracellular protein levels of these three isoforms in both vegatative and aggregation-stage cells, since large differences in the amounts of these isoforms could underlie results that suggest functional differences.

Materials and Methods

General Molecular and Cell Biological Methods

General molecular biological methods were performed as described in

1. *Abbreviations used in this paper*: DM, double mutant; ECL, enhanced chemiluminescence; SB, starvation buffer; TH, tail homology; TM, triple mutant.

Sambrook et al. (45) and, as they apply specifically to *Dictyostelium*, in Spudich et al. (49). To measure doubling times, cell concentrations were determined using a particle counter (Z1; Coulter Electronics Inc., Hialeah, FL) at 8–12-h intervals starting with early log-phase cells. Values were determined by fitting an expontial curve to the data for cell number vs. time. To perform streaming assays, midlog-phase cells in HL5 media were allowed to adhere for 1 h to tissue culture dishes (3003; Falcon Plastics, Cockeysville, MD) (0.5×10^6 cells per cm^2), and the media was changed to starvation buffer (SB) (20 mM KCl, 20 mM potassium phosphate, pH 6.6, and 2 mM $MgCl_2$). The development of cells on black filter supports was performed as described previously (18) using ~1-cm-diam spots containing $\sim 2 \times 10^6$ cells. SDS-PAGE was performed as described by Laemmli (25). Proteins were transferred to nitrocellulose using a semi-dry blotter (Millipore Corp., Bedford, MA). Western blots were developed using either ^{125}I protein A (New England Nuclear, Boston, MA) or an enhanced chemiluminescence (ECL) detection system (Amersham Corp., Arlington Heights, IL). The intensities of ^{125}I- and ECL-generated autoradiograms were determined using a laser densitometer (Pharmacia LKB, Piscataway, NJ) within the linear range of response.

Mutant Generation

The creations of the myoB$^-$ single mutant strain null 6 (by targeted gene disruption in axenic strain Ax3) and the myoD$^-$ single mutant strain LD14 (by targeted gene disruption in axenic strain HC6, an Ax2 derivative) were described previously (18, 21). To create myoB/myoD double mutants, two plasmids were designed to generate myoD antisense RNA within strain null 6. The G418^R vector BS18, which drives antisense RNA expression using the strong, constitutive ACT15 promoter, was cut with BglII and treated with phosphatase, yielding plasmid A. An ~2.4-kb EcoRI fragment of genomic DNA that contains ~260 bp of 5′ flank and the coding sequence for the NH_2-terminal 616 residues (~55%) of the myoD heavy chain was blunt-ended, converted to BamHI ends by linker addition, and cloned into plasmid A in the antisense orientation (yielding plasmid B). An ~1.5-kb EcoRI insert from a 3′ cDNA clone that contains the COOH-terminal 497 residues (~45%) of the heavy chain was blunt-ended, converted to BamHI ends, and cloned into plasmid A in the antisense orientation (yielding plasmid C). Plasmids B (head construct) and C (tail construct) were introduced by calcium phosphate–mediated DNA transfection as supercoiled DNA. Transformants were selected in high concentrations of G418 (80–100 μg/ml), purified by serial dilution (18), and examined by Western blot analysis using the myoD-specific antibody (21).

To create myoB/myoC/myoD triple mutants, a vector was designed for targeted disruption of the myoC gene within a representative double mutant strain, DM·4. The phleomycin^R vector pfDEI (gift of A. Noegel, Max-Planck Institute, Martinsried, Germany) was linearized with HindIII (which cuts just 5′ of the phleo^R cassette), blunt-ended, converted to ClaI ends, and treated with phosphatase (yielding plasmid D). A 1,604-bp PvuII fragment that contained nucleotides 288–1798 from a myoC genomic clone (34) (gift of M. Titus, Duke University, Durham, NC) plus 93 bp of pUC 18 was converted to ClaI ends and cloned into plasmid D in the same orientation as the phleo^R cassette. The resulting plasmid was cut with BamHI (which cuts just 3′ of the phleo^R cassette) and treated with phosphatase, yielding plasmid E. A 746-bp HindIII/PvuII fragment containing nucleotides 2370–3115 from the myoC gene was blunt-ended, converted to BamHI ends, and cloned into plasmid E in the same orientation as the phleo^R cassette, yielding plasmid F. DM·4 was transformed by electroporation with either supercoiled plasmid F (should integrate by a single crossover event as a long tandem repeat) or with plasmid F that had been cut with HindIII and EcoRI (should allow the integration of a single copy of the linear disruption fragment by a double-crossover, gene replacement event). Transformants were selected in 20 μg/ml phleomycin (Cayla Inc., Toulouse, France), purified, and examined by Southern blot analysis and by Western blot analysis using the myoC-specific antibody.

To create myoC$^-$ single mutants, a vector was designed for targeted disruption of myoC in the thymidine auxotroph, JH10 (gift of R. Firtel, University of California at San Diego). To create this vector, the ~1.5-kb phleo^R cassette in plasmid F above was removed by digestion with XbaI and replaced with a 3.3-kb THY cassette. JH10 cells were transformed by electroporation with the linear disruption fragment, following its release using HindIII and EcoRI, and were selected in unsupplemented HL5 media.

All cells were grown in complete HL5 media, pH 6.6, with the following additions: (*a*) tetracycline (12.5 μg/ml) and ampicillin (50 μg/ml), (all strains); (*b*) thymidine (0.5 mg/ml for JH10 cells); (*c*) G418 (20 μg/ml for myoB$^-$ and myoD$^-$ single mutants and 80 μg/ml for double and triple mutants; and (*d*) phleomycin (20 μg/ml for triple mutants). For routine maintenance of triple mutants, HL5 media was adjusted to pH 7.3 to increase drug efficacy. All experiments were performed in regular HL5 media, pH 6.6. Drugs were usually included since several assays (e.g., growth rates and pinocytosis) yielded the same results with and without drugs. Finally, (*a*) antisense cell lines were deemed to be homogeneous based on immunofluorescence staining; and (*b*) the double and triple mutant strains examined in detail are unequivocally independent transformants since they were isolated from separate transformation plates.

Motility Measurements

To measure the speed of aggregation-competent cells undergoing random walks, cells were developed on black filter supports to "ripple stage," gently washed off the filter pad with SB buffer, and rapidly diluted to $\sim 1 \times 10^5$ cells per ml. This suspension was perfused into a Dvorak-Stotler chamber (Nicholson Precision Instruments, Inc., Gaithersburg, MD), and the cells were allowed to adhere to the top coverslip (5 min). The chamber was then inverted and placed on the stage of an upright microscope (Axioplan; Carl Zeiss, Inc., Thornwood, NY). SB buffer was continuously perfused through the chamber during experiments at a rate of 10 ml/h using a syringe pump (55-3333; Harvard Apparatus Co., South Natick, MA). This perfusion rate, which results in the complete exchange of the solution in the chamber every ~80 s, combined with the low density of cells in the chamber, serves to prevent cell–cell communication via cAMP signaling (61). Bright-field images (×10) were magnified with a ×4 lens and captured using a Newvicon video camera (C2400-07; Hamamatsu Corp., Middlesex, NJ). Time-lapse images were recorded for 10 min using an optical disc recorder (TQ-303IF; Panasonic, Secaucus, NJ) at a sampling rate of 5 s. This very short time interval is required for the accurate measurement of cell speeds for slow strains that exhibit little directional persistence (Wu, X., and J.A. Hammer, unpublished observations). Video image series were sent to a Macintosh Quadra 950 computer for image processing via a Data Translation QuickCapture digitizing board. Cell motion analysis was performed using DIAS software (Dynamic Image Analysis System; SoilTech Inc., Iowa City, IA). Image sequences were first automatically digitized to obtain the outlines of cell perimeters by a user-specified gray level threshold. The centroid locations of all cells for the sequence were computed first, and then the path of the centroids over time for each cell was determined. Any cell path involved in aggregations or collisions of two cells was removed from further analysis. The speed of centroid translocation was calculated using the central difference method, which is defined as the displacement between centroids before and after the current frame divided by the time intervals between the two frames. The average values of the centroid speeds over the 10-min observation period were used for quantitative evaluation of cell motility rate. On average, each experiment yielded usable data for six to eight cells. The noise level of the system was measured as 0.3 μm/min by examining nonmoving polystyrene spheres embedded in 1% agarose. Therefore, cells having speeds of $<\sim 0.5$ μm/min, which represented <3% of the total number of cells viewed, were removed from further analysis.

Pinocytosis

To measure the rate of fluid phase pinocytosis, cells were incubated in complete HL5 media in the presence of 2 mg/ml FITC-dextran (average mol wt 71,000) (No. FD-705; Sigma Chemical Co., St. Louis, MO). Unless indicated otherwise, assays were performed in shaking suspension culture (150 rpm) (orbital shaker, model 3520; Lab-Line Instruments, Inc., Melrose Park, IL) at 21°C and at a density of 5×10^6 cells per ml. Samples (2 ml) were mixed with 4 ml ice-cold Sorensen's phosphate buffer to rapidly stop pinocytosis. All subsequent steps were performed at 4°C. Uningested dextran was separated from ingested dextran by centrifugation of cells through an 8-ml cushion of PEG 8000 in Sorensen's buffer (1,500 rpm, 10 min) (RC6000 B; Sorvall Instruments Div., Newton, CT) (22, 59). All of the uppermost layer and about half of the cushion were aspirated, the walls of the tube were rinsed three times with Sorensen's buffer (with aspiration in between each wash), the sample was spun again (3 min), and the remainder of the cushion was aspirated. The cell pellet was resuspended in 750 μl of 50 mM sodium phosphate, pH 9.2, and lysed by addition of 750 μl of the same buffer containing 0.4% Triton X-100. Fluorescence intensities were measured using excitation and emission wavelengths of 485 and 520 nm, respectively. Variations in the number of cells in the final pellets, due to sampling/processing errors and to the

markedly different doubling times that these strains possess, were corrected for by measuring the amount of whole cell protein in each final sample (Bio-Rad Laboratories, Richmond, CA) and adjusting the fluorescence intensities accordingly. The amounts of cell-associated fluorescence were converted to μl of media accumulated based on the concentration of fluorescence in the media.

To measure transit times and efflux kinetics, cells were incubated as above in FITC-dextran (10 mg/ml) for 7.5 min, rapidly separated at 4°C from uningested dextran as above, washed once in cold HL5 media, resuspended at ~5 × 10^6/ml in 21°C HL5 media (without dextran), and incubated in shaking culture. To determine the amount of cell-associated dextran remaining in the cells over time, 1.5-ml samples were spun at 4°C in a microfuge (90 s), the pellet resuspended as above, and the amounts of whole cell protein and the fluorescence intensity measured.

To measure the rates of pinocytosis for cells attached to a surface, each time point consisted of ~5 × 10^6 cells adhered to a 60-mm tissue-culture dish (3002; Falcon Plastics). At the appropriate times, the media containing uningested FITC-dextran was aspirated, the cells were washed rapidly and gently with HL5 media (1×) and Sorensen's buffer (2×), released into 1.2 ml of Sorensen's buffer with a cell scraper, and processed as for the efflux experiments above. Finally, to photograph cells loaded with a fluid phase marker, dextran coupled to Texas red (No. 1002; Sigma Chemical Co.) was used because of its resistance to quenching by low pH.

Phagocytosis

The initial rate of uptake of plain, FITC-conjugated, monodisperse 1-μm polystyrene latex beads (No. 17154; Polysciences, Inc., Warrington, PA) was determined by a modification of the method of Vogel (59). Experiments were performed in shaking suspension culture in complete HL5 media (prefiltered through a 0.2-μm filter) at 110 rpm on an orbital shaker. *Dictyostelium* and beads were used at 5 × 10^6/ml and 2 × 10^9/ml, respectively, since this ratio of cells to beads (1:400) yielded maximal initial rates of uptake. Samples (2 ml) were mixed with 4-ml ice-cold Sorensen's phosphate buffer to rapidly halt phagocytosis. All subsequent steps were performed at 4°C. Uningested beads were separated from ingested beads by centrifugation of cells through a PEG cushion exactly as described above. The cell pellet was resuspended in 1 ml of 50 mM sodium phosphate, pH 9.2, lysed by the addition of 1 ml of the same buffer containing 0.4% Triton X-100, and fluorescence intensities were measured as described above. Sampling variations were corrected for by determination of whole cell protein in each sample (Bio-Rad assay). Conversion of relative fluorescence intensity to actual numbers of beads ingested was done using a standard curve of fluorescence vs. known numbers of beads. Measurements performed with Ax3 cells at 4°C (where phagocytosis is blocked, but attachment is not) indicated that centrifugation through the PEG cushion strips attached as well as uningested beads from the cells. For the bead efflux experiments, Ax3 and triple mutant cells were fed beads for 2.5 min, separated from uningested beads, incubated in media without beads, and the amount of cell-associated fluorescence measured at various time intervals.

Antibodies

The generations of the isoform-specific, rabbit polyclonal antibodies to myoB and myoD were reported previously (18, 21). The α myoB antibody was further purified by repeated adsorption against myoB$^-$ whole cell extracts exactly as described previously for the α myoD antiserum (21). To generate a myoC-specific antibody, a 746-bp DraI fragment from the myoC heavy chain gene (nucleotides 2,910–3,655), which encodes residues 934–1,153 or ~60% of the tail domain, was EcoRI-linkered and cloned into the glutathione S-transferase fusion vector pGEX-3X (Pharmacia LKB). Expression in *Escherichia coli* strain HB101 and purification of the ~50-kD fusion protein on glutathione–Sepharose were performed according to the manufacturer's instructions. Rabbit immunizations and the purification of the crude myoC antiserum by repeated adsorption against myoC$^-$ whole cell extracts were performed exactly as described previously (21).

Immunofluorescence

The localization of myoC was performed using the cell flattening (agar overlay) and fixation techniques of Fukui et al. (10). To generate fields of oriented, migrating cells, JH10 cells were cultured in HL5 media within chamber slides (Nunc, Roskilde, Denmark), switched to starvation buffer, and allowed to commence chemotactic aggregation (streaming). At this time they were briefly overlaid with the agar sheet, fixed, and stained (as described in reference 21) with a 1:10 dilution of the purified α myoC antibody (which represents a ~400-fold dilution relative to the crude antiserum). FITC-labeled goat anti–rabbit antibody (Jackson ImmunoResearch Laboratories, Inc., Avondale, PA) was used as the secondary antibody. Images were obtained on a Zeiss Axioplan microscope using a ×63 Planapo phase 3 objective, a camera (MC 100; Carl Zeiss, Inc.), and film (T-MAX 400; Eastman-Kodak Co., Rochester, NY).

Quantitation of Protein Levels

Standard curves that contained 100–1,000 pg (in increments of 100 pg) of the three purified fusion proteins used to raise the isoform-specific antibodies to myoB (18), myoC, and myoD (21), and aliquots of whole cell extracts from vegetative Ax3 cells that contained between ~300–600 pg of each isoform (determined from pilot experiments), were resolved by SDS-PAGE, transferred to nitrocellulose, and probed with the purified antibodies to myoB, myoC, and myoD. The blots were developed using an ECL detection system, and autoradiograms in which the lowest standard was just visible to the eye were scanned using a laser densitometer. The slopes of the standard curves, which were linear under these conditions, were used to calculate the amounts of each isoform per 10^6 vegetative cells. Corrections for the weight differences between the fusion protein standards and the intact heavy chains were included in the calculations.

Results

MyoC Localizes to the Leading Edge of Migrating Cells

MyoB and myoD have previously been shown to be concentrated within actin-rich pseudopods at the leading edge of migrating cells (10, 21). To determine if myoC has a similar localization, we used an approach described previously (21) to create a myoC-specific polyclonal antibody. Because this approach requires the use of a myoC$^-$ null cell line, initial efforts were directed at creating such a cell line. To accomplish this, a linear disruption fragment was generated that contained ~1.6- and ~0.75-kb pieces of the myoC gene with the 3.3-kb THY cassette in between (Fig. 1, *bottom*). This fragment was introduced into the thymidine auxotroph JH10 by electroporation, and transformants were selected in unsupplemented media. Fig. 1 (*bottom*) shows the changes in the structure of the endogenous gene that should result from the expected double-crossover, gene replacement event. Such recombinants were identified in Southern blots (Fig. 1, *top*) based on (*a*) a shift in the size of the BclI fragment that spans most of the myoC gene (from ~5.4 to ~8.2 kb; identified using probe A) and (*b*) the absence of cross-reaction between this ~8.2-kb BclI band and probe B (which corresponds to the ~570-bp portion of the gene that would be lost from the genome).

To generate and purify the myoC-specific antiserum, a polyclonal antibody was raised against a glutathione-S-transferase/myoC fusion protein containing ~60% of the myoC tail domain. The crude antiserum reacted strongly in whole cell extracts of JH10 cells with an ~125-kD band corresponding in size to the myoC heavy chain, as well as with several other bands (Fig. 2, lane *4*). The antibodies that react with these additional proteins were removed by repeatedly absorbing the serum against nitrocellulose membranes to which extracts from myoC$^-$ cells had been bound. The resulting antiserum reacts only with the ~125-kD polypeptide (Fig. 2, lane *5*). Proof that this polypeptide is the myoC heavy chain and that the antise-

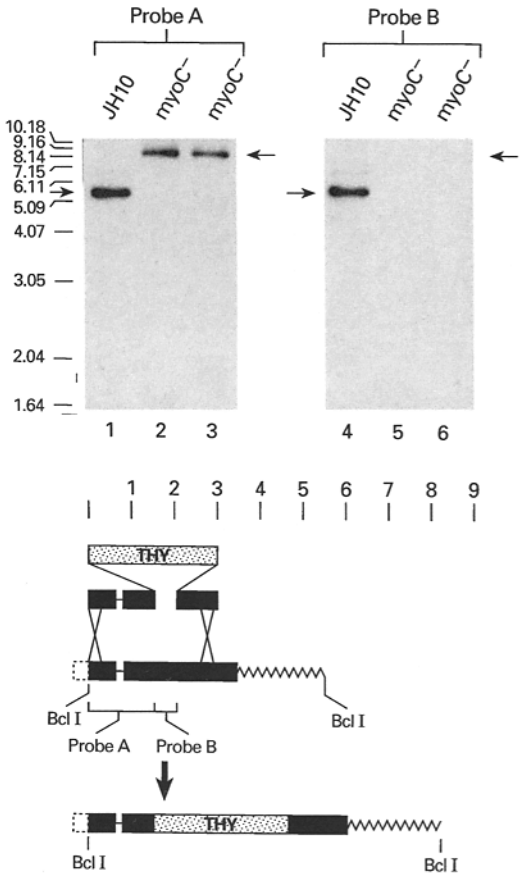

Figure 1. Targeted disruption of the myoC heavy chain gene. The schematic at the bottom shows the design of the linear disruption vector, the positions of probes A and B, and the change in the structure of the myoC gene in the event of a double-crossover, gene replacement event. This change was confirmed by Southern blot analyses using probe A (*upper left*), which detected a shift in the size of the BclI band from ~5.4 kb in Ax3 cells (lane *1*) to ~8.2 kb in myoC⁻ cells (lanes *2* and *3*), and probe B (*upper right*), which detected the ~5.4 kb band in Ax3 cells (lane *4*), but not the ~8.2 kb BclI band in myoC⁻ cells (lanes *5* and *6*). Lanes *2* and *5* correspond to the myoC⁻ clone LC16.

rum is specific for this isoform was obtained by probing extracts of myoC⁻ cells (Fig. 2, lane *6*). The purified α-myoC antiserum clearly does not recognize the other myosin I isoforms expressed in myoC⁻ cells.

To localize the myoC isoform, fields of oriented, migrating JH10 cells were prepared as described in Materials and Methods and stained with the myoC-specific antibody (Fig. 3). Virtually every cell in all three fields shows intense staining for myoC at the leading edge. This localization corresponds to phase dense pseudopods at the leading edge, which are known to be composed of a dense F-actin meshwork (10,35,43). The staining of myoC⁻ cells under identical conditions was completely negative (data not shown). While it remains to be seen whether myoC localizes to other actin-rich regions where myoB and myoD localize (e.g., sites of cell–cell contact, filopodia), in one important way myoC colocalizes with myoB and myoD. Therefore, these three classic myosin I isoforms appear to be closely related not only in terms of tail domain structure, but also in terms of localization in migrating cells.

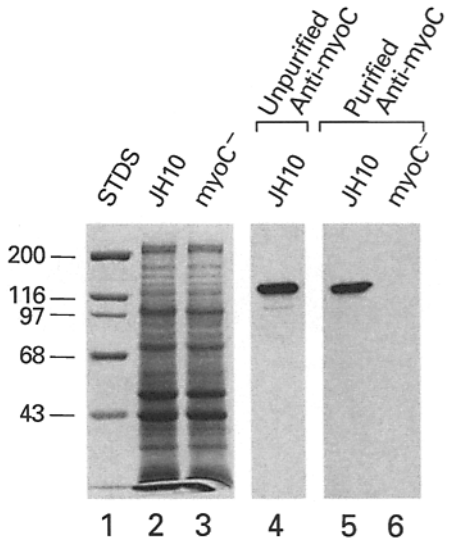

Figure 2. Purification and characterization of the myoC-specific antibody. Lanes *1–3* are Coomassie blue–stained standards and whole cell extracts from control JH10 cells and a myoC⁻ cell (LC16), respectively. Lanes *4–6* are ECL Western blots of whole cell extracts of JH10 cells (lanes *4* and *5*) and myoC⁻ cells (lane *6*) that were probed with either the crude α myoC antibody (lane *4*) or the purified α myoC antibody (lanes *5* and *6*).

Of MyoB⁻, MyoC⁻, and MyoD⁻ Single Mutants, Only MyoB⁻ Cells Exhibit a Significant Reduction in the Speed of Whole Cell Translocation

Wessels et al. (61) previously found that aggregation-stage myoB⁻ cells undergoing random walks crawl at 51% of the rate of their parental control, Ax3 (Ax3, 10.1 ± 2.8 μm/min [n = 22]; myoB⁻, 5.2 ± 3.6 μm/min [n = 20]; $P <$ 0.05). To determine whether myoC and myoD also play a significant role in cell locomotion, the average speed of aggregation-stage myoC⁻ cells (line LC16) and myoD⁻ cells (line LD14) (21) was determined. As a point of reference, the speed of ripple-stage myoB⁻ cells (line null 6) (19) was again measured. The speeds of the appropriate control strains (Ax3 for myoB⁻ cells, JH10 for myoC⁻ cells, and HC6 for myoD⁻ cells) were also measured. Briefly, these six cell lines were starved on black filter supports to ripple stage, disaggregated, seeded in a Davorak-Stotler perfusion chamber, and the rate of whole cell translocation was determined from time-lapse video microscopic images using DIAS software (48) (Table I). MyoB⁻ cells were again found to crawl significantly slower (44% slower) than their parental cell line, Ax3. MyoC⁻ and myoD⁻ cells, on the other hand, were not significantly different than their parental control strains.

Only MyoB Protein Levels Are Strongly Upregulated During Early Development

The above results suggest that myoB has a more important role than myoC and myoD in the motility of migrating, aggregation-stage cells. ECL Western blot analyses of developing cells using the isoform-specific antibodies to myoB, myoC, and myoD are consistent with this proposal (Fig. 4). Specifically, the amount of myoB heavy chain rises progressively and dramatically during early aggregation,

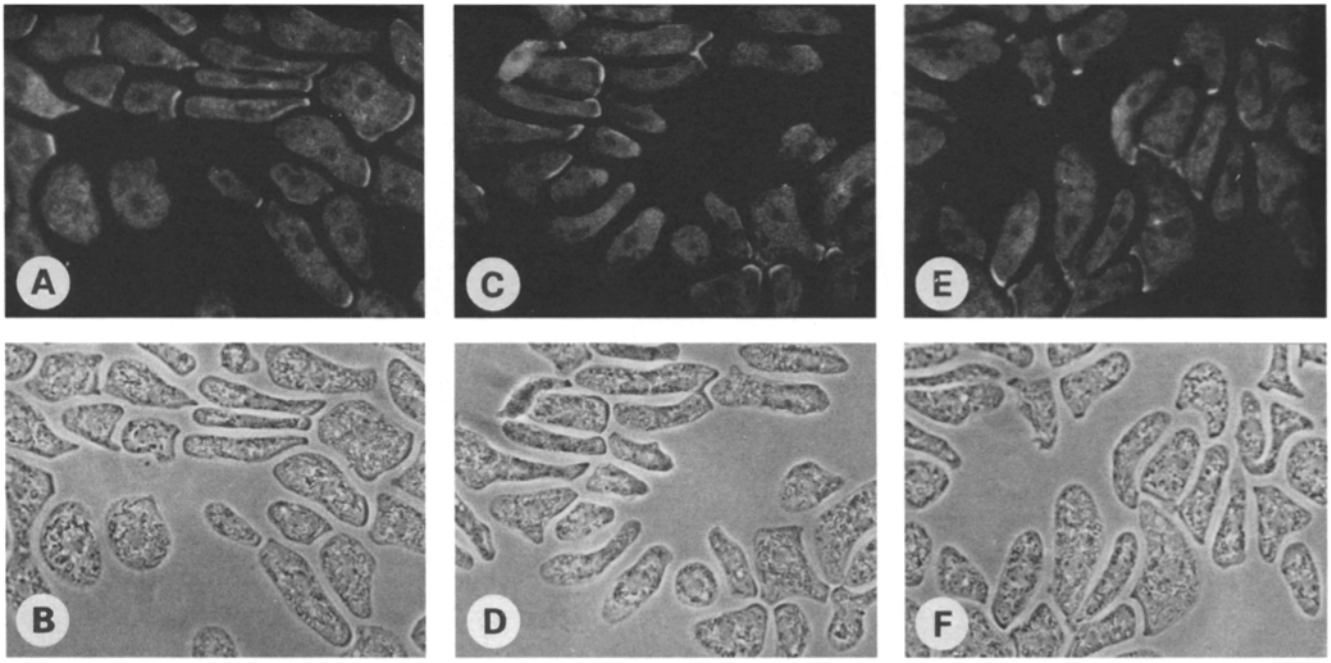

Figure 3. Immunofluorescence localization of myoC in migrating cells. Shown are phase contrast (*B*, *D*, and *F*) and fluorescent (*A*, *C*, and *E*) images of fields of JH10 cells that were undergoing chemotactic aggregation and were stained with the myoC-specific antibody. The cells were moving primarily toward the right in *B* and *D* and toward the lower left side in *C*.

reaching a value at ripple stage (when motility measurements were made) that is about six times higher than in vegetative cells (Fig. 4 *B*). By contrast, the amounts of both the myoC and myoD heavy chains remain essentially unchanged during early development.

*Table I. Speeds of Aggregation-stage Cells Undergoing Random Walks**

Strain	Average speed‡§	
	μm/min	*n*
Ax3	11.01 ± 4.39	44
NULL6	6.17 ± 3.12	50
DM·2	5.53 ± 2.55	23
DM·4	3.93 ± 2.40	34
TM·1	3.89 ± 2.01	31
TM·2	3.04 ± 1.89	38
JH10	8.26 ± 4.05	44
LC16	9.96 ± 6.43	48
HC6	10.73 ± 6.27	51
LD14	9.90 ± 6.43	44

*The distributions of the speeds for all these cell lines were essentially unimodal. Therefore, none of the average speeds represent a mixture of two or more subpopulations of cells with obviously different speeds.

‡ Shown is the mean ± SD.

§ For determination of significance, the *t* test was used, and only strains with the same parental line were compared (e.g., Ax3, Null6 [myoB$^-$],DM·2, DM·4, TM·1, and TM·2 were compared; JH10 and LC16 [myoC$^-$] were compared; and HC6 and LD14 [myoD$^-$] were compared). Ax3 cells were significantly different ($P < 0.05$) from all five mutants derived from it. Null6 cells were significantly different from all strains except DM·2. DM·2 cells were significantly different from all strains except Null6. DM·4 cells were significantly different from all strains except TM·1 and TM·2 (which were derived from it). TM·1 and TM·2 cells were significantly different from all strains except DM·4 and each other. LC16 cells were not significantly different from JH10 cells, and LD14 cells were not significantly different from HC6 cells.

The Absolute Amount of MyoB in Aggregation-stage Cells Is Also Much Higher Than the Amounts of MyoC and MyoD

While the above results support the idea that the cells place a special demand on the myoB isoform during the time that they become highly motile, it is possible that myoC and myoD also contribute to whole cell motility, but that their contributions are less obvious because they are present at lower levels than myoB. To determine the absolute amounts of myoB, myoC, and myoD proteins in the cell, ECL Western blots of *Dictyostelium* whole cell extracts (vegetative cells) were compared with blots of known amounts of the *E. coli* fusion proteins used to raise the three isoform-specific antibodies. The values obtained were 8.00 ± 0.56 ng/10^6 cells for myoB, 6.30 ± 0.98 ng/10^6 cells for myoC, and 2.51 ± 0.17 ng/10^6 cells for myoD (n = 5). These results indicate, therefore, that in vegetative cells there is ~1.3 and ~3.2 times more myoB than myoC and myoD, respectively. Moreover, using the relative expression data in Fig. 4, we calculate that ripple-stage cells contain ~6 and ~16 times more myoB than myoC and myoD, respectively. These results suggest, therefore, that the lack of a significant reduction in cell speed for myoC$^-$ and myoD$^-$ mutants at ripple stage may reflect their low abundance, rather than functional differences from myoB.

Double and Triple Mutants of These Three Classic Myosin I Isoforms Show Only a Small Additional Impairment of Whole Cell Motility

While the myoC$^-$ and myoD$^-$ single mutants do not exhibit significant reductions in the rate of cell translocation, it is possible that suppression of the levels of these two iso-

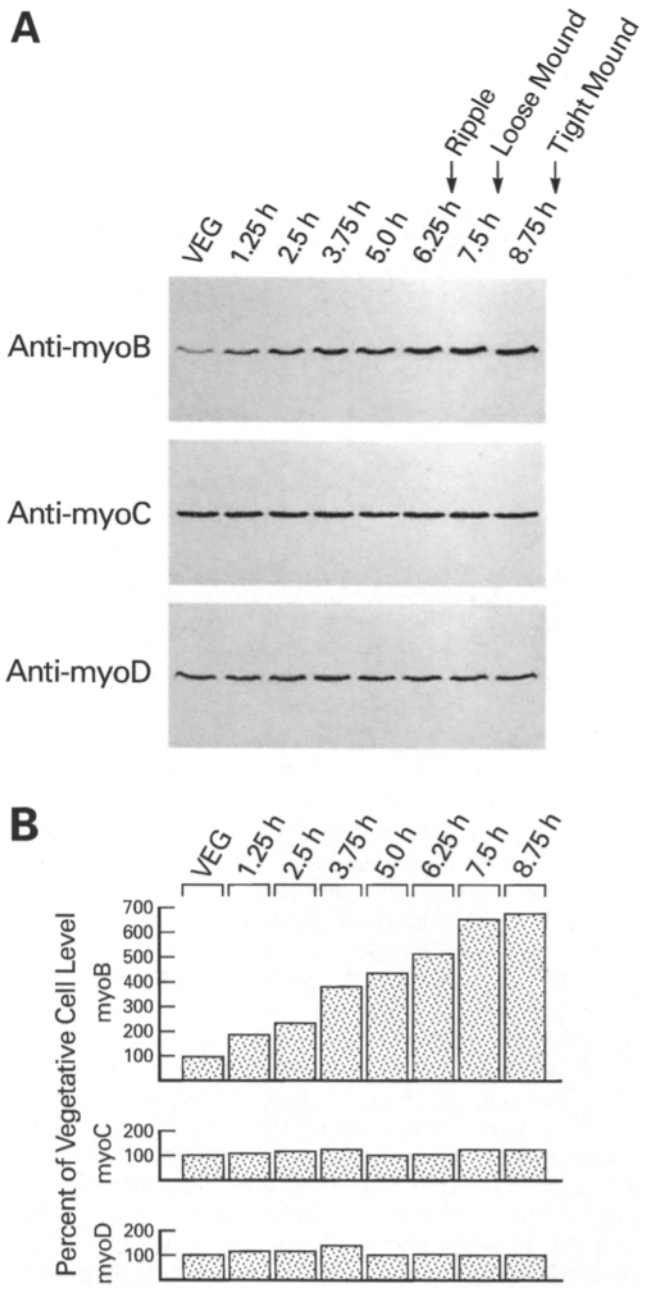

Figure 4. Developmental expression of myoB, myoC, and myoD protein isoforms. Ax3 cells were developed on black filter supports for the indicated times and harvested in SB buffer. Replicate samples of whole cell extracts (prepared as described previously [18] and corrected for slight differences in the numbers of cells per sample based on protein measurements [Bio-Rad Laboratories]) were subjected to ECL-based Western blot analyses using isoform-specific antibodies to myoB, myoC, and myoD (*A*). *B* shows the levels of these three isoforms as a percentage of vegetative cell levels, based on laser densitometric measurements within the linear response range. The times at which the cultures reached ripple, loose mound, and tight mound stages are shown. *VEG*, vegetative cells.

forms in a myoB$^-$ background might lead to further and significant decreases in cell speed. To look for such synergistic effects, we created and analyzed myoB/myoD double mutants and myoB/myoC/myoD triple mutants.

To create myoB/myoD double mutants, the myoB$^-$ strain null 6 was transformed separately with two plasmid constructs designed to suppress myoD protein levels via constitutive expression of antisense RNA[2]. Fig. 5 shows an autoradiogram of a Western blot developed using the myoD-specific antiserum (21) and I^{125} protein A for four independent myoB$^-$/myoD antisense double mutant (DM) cell lines. DM·1 and DM·2 were obtained using the head construct, while DM·3 and DM·4 were obtained with the tail construct (see Methods and Materials). Scanning of the autoradiograms revealed >99.8% suppression of myoD in DM·1–DM·4. This suppression was constant over continuous culture (Fig. 5) and across early development (data not shown).

To create myoB/myoC/myoD triple mutants (TM), strain DM·4 was transformed with a phleomycin resistance vector that was designed to disrupt the myoC heavy chain gene by a double-crossover, gene replacement event. Transformations were performed separately with both the linearized disruption fragment and the closed, supercoiled plasmid. Southern blots revealed that the myoC gene was not disrupted in any of the ~80 purified clonal isolates selected in the presence of phleomycin. Nevertheless, in many of the clonal isolates transformed with supercoiled plasmid DNA (which by Southern analysis contained ~50–100 integrated copies), myoC heavy chain protein levels, as accessed by ECL Western blots using the myoC-specific antiserum described above, were very low (Fig. 6). In some isolates (e.g., TM·1 and TM·2), myoC levels were <0.2% of Ax3 (and DM·4) levels. MyoC suppression was constant across early development and myoD antisense suppression was also retained in these triple mutant isolates (data not shown).

The mechanism by which the level of myoC heavy chain protein was suppressed was revealed by a series of Northern blots. First, blots performed with double-stranded myoC probes (Fig. 7 *A*) showed that the normal ~4-kb myoC RNA is virtually absent in the best TM isolates (e.g., TM·1 and TM·2), and in its place is a heterogeneous population of RNAs ranging in size from ~6–8 kb. Second, these latter RNAs were found to hybridize specifically with probes that recognize only the antisense strand (Fig. 7 *B*). Therefore, the suppression of myoC protein levels is most likely due to an antisense effect, even though the vector was not designed specifically for this purpose. While the antisense suppression of myoC is stable in continuous culture over a period of weeks, it is not so over a period of months (myoC levels gradually rise over long-term culture to a level of ~10% of wild type). Therefore, for all experiments, fresh TM cultures were used (i.e., grown for <1 mo from frozen stocks of the original trans-

2. Efforts to create myoB/myoD double mutants by targeted disruption of the myoD heavy chain gene in null 6 were complicated by the fact that null 6 (and the original parental strain Ax3) appear to contain two functional copies of the *myoD* gene. The existence of these two copies, which are indistinguishable in fairly detailed restriction enzyme maps, may be due to a recent chromosomal duplication. The consequence of this apparent duplication was that, while numerous homologous recombinants were obtained, in all of them only one of the two myoD heavy chain genes was disrupted, and all of these cell lines expressed near normal levels of the myoD heavy chain polypeptide. To circumvent this problem, we used the antisense approach.

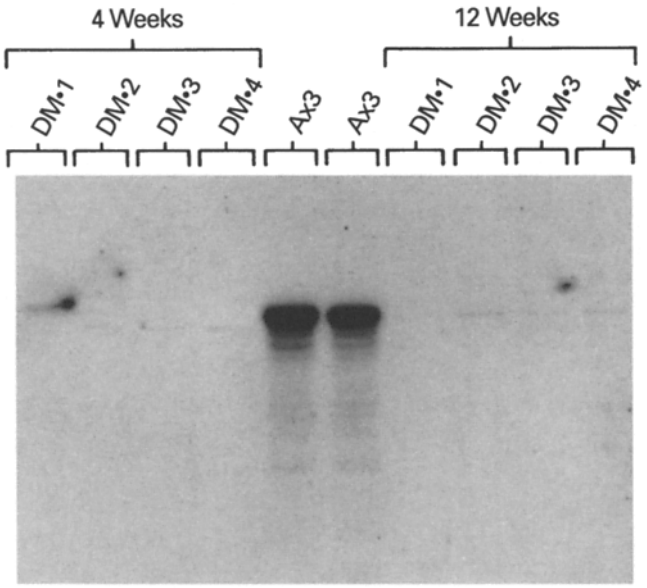

Figure 5. Suppression of myoD protein levels in myoB⁻/myoD antisense DM strains. Shown is an autoradiogram of a Western blot of whole cell extracts (1×10^6 cells per lane) from Ax3 cells and four independent DM strains at 4 and 12 wk of continuous culture. The blot was probed with the myoD-specific antiserum (21) and was developed using I^{125}–protein A. The smudge in the left most lane is an artifact. Southern blots of all four cell lines revealed that the myoD genes are unperturbed (data not shown), indicating that these are true antisense cell lines for myoD.

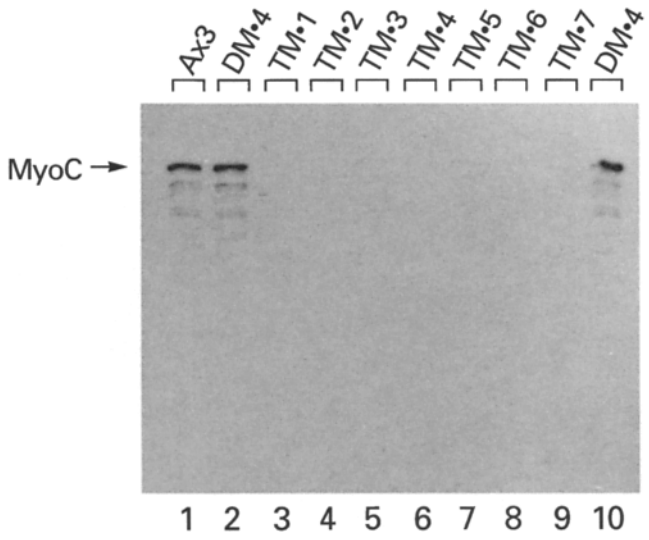

Figure 6. Suppression of myoC protein levels in myoB⁻/myoD antisense/myoC antisense TM strains. Shown is an ECL Western blot of whole cell extracts (0.8×10^6 cells per lane) from Ax3 (lane *1*), DM·4 (lanes *2* and *10*), and seven independent TM strains (lanes *3–9*). The blot was probed with the myoC-specific antibody.

formants), and myoC levels on the day of the experiment were checked to be sure that they were low (<2%).

Table I shows the results of motility measurements for double mutant strains DM·2 and DM·4 and triple mutant strains TM·1 and TM·2 at ripple-stage[3]. Of the two DM strains, only one (DM·4) was significantly slower (34% slower) than its most immediate parental strain, null 6. Furthermore, neither of the two TM strains were significantly slower than their immediate parental strain, DM·4. These results indicate that the near complete suppression of two additional classic myosin I isoforms in a myoB⁻ mutant has only a small additional effect on whole cell motility.

MyoC, Like MyoB, Plays a Role in Supporting Efficient Streaming Behavior, but Its Role Is Evident Only in the Double Mutant Background

When *Dictostelium* cells are seeded in dishes at relatively low density in nonnutrient buffer, they aggregate in a process driven by chemotaxis towards cAMP. They initially migrate as single cells but migrate later as streams of cells attached head to tail (49). The streaming process, which begins in ~6 h for Ax3 cells, ends within ~12–14 h in the formation of a tight aggregate containing ~100,000 cells.

3. While the streaming behavior of TM cells was strikingly impaired (see Fig. 8), they were able to aggregate on black filters (where the initial cell density is ~30 times higher than in streaming assays) and complete development, although they reached ripple stage in ~9 h, as compared to ~7 h for Ax3 cells.

We found previously that myoB⁻ cells take longer to initiate streaming and, once they begin the process, ~1.5 times longer to form tight aggregates (18). This reduction in streaming efficiency may be a behavioral consequence of the slower rate of cell locomotion exhibited by aggregation-stage myoB⁻ cells (61) (Table I). Consistent with this, myoC⁻ cells and myoD⁻ cells, which are both indistinguishable from wild type in terms of the speed of ripple-stage cells (Table I), are also both normal in terms of streaming efficiency (21,34, unpublished observations).

To look for possible synergistic effects between these three isoforms, the streaming behaviors of double and triple mutants were analyzed. Fig. 8 shows typical streaming behavior for Ax3 cells and various mutant strains at 10, 12.5, and 15 h. Strain DM·4 was not obviously worse than myoB⁻ cells, exhibiting approximately the same degree of impairment in streaming efficiency relative to Ax3 cells as do myoB⁻ single mutants (see reference 19). By contrast, strains TM·1 and TM·2 formed very small streams and aggregates such that their streaming behavior was dramatically impaired relative not only to Ax3 cells, but also to DM·4 cells. Evidence that the additional impairment exhibited by TM·1 and TM·2 was in fact due to the suppression of myoC protein levels was obtained by analysis of strain TM·C. The streaming behavior of these cells, which are phleomycin resistant but express essentially normal levels of myoC heavy chain protein (data not shown), was indistinguishable from that of DM·4 cells (Fig. 8). Because the suppression of myoC protein levels in a myoB/myoD double mutant background appears to have a much greater effect on streaming behavior than on the speed of cells, we conclude that the role of myoC in supporting streaming behavior does not primarily involve powering whole cell motility. Whatever role this is, it is only apparent in the DM background. Therefore, either the function of myoC is compensated for in the myoC⁻ single mutant,

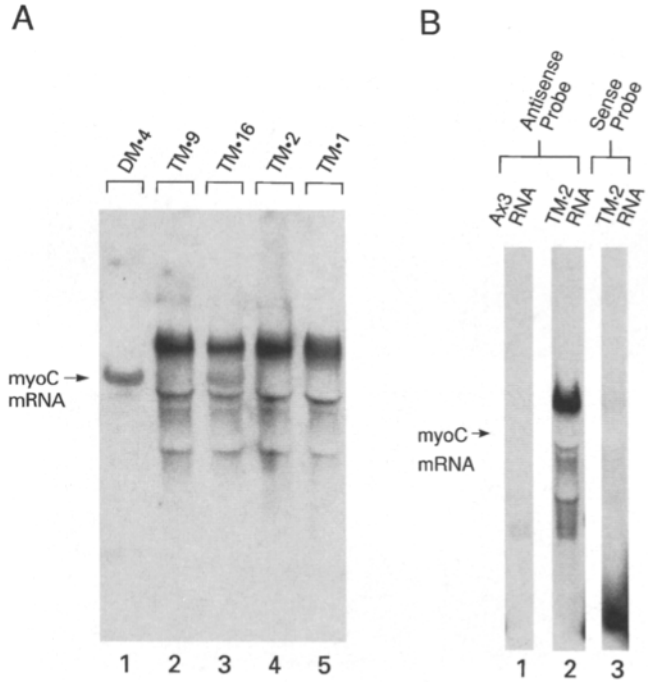

Figure 7. Northern blots reveal the mechanism by which myoC protein levels are suppressed in triple mutant strains. (*A*) Total RNAs from DM·4 cells (lane *1*) and TM strains that contain either significant levels of myoC protein (~5–30% of wild type) (lanes *2* and *3*) or very low levels of myoC protein (<1% of wild type) (lanes *4* and *5*) were probed at high stringency with a myoC-specific, double-stranded DNA probe. (*B*) Total RNAs from Ax3 cells (lane *1*) and TM·2 cells (lanes *2* and *3*) were hybridized at high stringency with myoC probes that were specific for either the antisense strand (lanes *1* and *2*) or the sense strand (lane *3*). Ax3 cells lack the antisense RNA, while TM·2 cells lack sense RNA of the correct size and contain a large amount of antisense RNA in the ~6–8-kb range.

and/or the striking effects seen here in TM strains are the result of synergism.

Both MyoB⁻ and MyoC⁻ Single Mutants Are Impaired in Phagocytosis, but Their Effects Are Not Additive

MyoB⁻ single mutants were previously shown to exhibit an ~32% reduction in the initial rate of uptake of FITC-labeled *E. coli* by phagocytosis (18). To determine whether myoC and myoD also play roles in phagocytosis, the initial rate of uptake of fluorescent 1-μm polystyrene beads was determined for myoC⁻ and myoD⁻ cells, together with their parental control strains. As a point of reference, myoB⁻ and Ax3 cells were again assayed. As in the previous study (18), myoB⁻ cells exhibited an ~37% reduction in the initial rate of phagocytosis (Fig. 9 *A*). Similarly, myoC⁻ cells exhibited an ~36% reduction (Fig. 9 *B*). By contrast, myoD⁻ cells were not obviously impaired in bead uptake (Fig. 9 *C*). Consistent with this, the rates of bead uptake exhibited by strains DM·2 and DM·4 were essentially identical to that of myoB⁻ cells (Fig. 9 *A*). Somewhat surprising, however, was the fact that the kinetics exhibited by strains TM·1 and TM·2 were also indistinguishable from that of myoB⁻ cells (Fig. 9 *A*). Therefore, while the analysis of myoB⁻ and myoC⁻ single mutants indicates that both isoforms play significant and nonredundant roles in supporting phagocytosis, analyses of triple mutants indicate that their functions are not additive.

Double and Triple Mutants Exhibit Significant Decreases in Doubling Time

During the process of passaging cells, our clear impression was that double mutants, and especially triple mutants, divided more slowly than Ax3 cells. To confirm this impression, the doubling times for all of the strains discussed above were determined in shaking culture during logarithmic growth (Table II). While the doubling times for all three single mutants were essentially indistinguishable from their parental controls, the doubling times for strains DM·2 and DM·4, and, in particular, strains TM·1 and TM·2, were much longer. Specifically, the doubling times of DM·2 and DM·4 were ~20% longer than for both Ax3 and null 6, their immediate parental strain. Furthermore, the doubling times of TM·1 and TM·2 were ~48% longer than for Ax3 and ~23% longer than for DM·4, their immediate parental strain. The longer doubling times exhibited by TM·1 and TM·2 relative to DM·4 are almost certainly due to the near complete suppression of myoC protein levels in the DM background, since strain TM·C has a doubling time that is indistinguishable from that of strain DM·4 (Table II). We calculate that if equal amounts of strains TM·1 (or TM·2) and Ax3 were mixed together and then grown in culture, Ax3 would comprise >99.8% of the culture in only ~10 d.

Single, Double, and Triple Mutants Exhibit Progressively Greater Decreases in the Rate of Uptake of a Fluid Phase Pinocytic Marker, and the Effects are Synergistic

In axenic culture, *Dictyostelium* cells derive their nutrients solely by means of engulfing media via pinocytosis (49). The slower growth rates exhibited by DM and TM strains might be due, therefore, to slower rates of fluid phase pinocytosis. To measure the kinetics of this process, which is constitutive in axenic strains of *Dictyostelium* (49), we used FITC-dextran, which has previously been shown to be an appropriate fluid phase pinocytic marker in this organism (22, 49). Fig. 10 *A* shows the kinetics of accumulation of FITC-dextran for Ax3 cells and the mutants that were derived from it (null 6, DM and TM strains), while *B* and *C* show the kinetics for myoC⁻ cells (vs. JH10) and myoD⁻ cells (vs. HC6), respectively. All of the measurements were made with cells growing in suspension culture in complete HL5 media. Furthermore, all of the values were corrected for differences in the amount of cell protein in the actual samples. This is especially important since the differences in doubling times between the strains are sufficiently large as to have significant differential effects on cell number over the time course of these experiments.

The results for Ax3 cells (as well as JH10 and HC6) closely resembled those reported by others (1, 22, 32, 41). Specifically, the accumulation of FITC-dextran in Ax3 cells increased in an essentially linear fashion over the first ~60 min, began to plateau by ~90 min, and reached a clear plateau by ~120 min. Others have shown conclu-

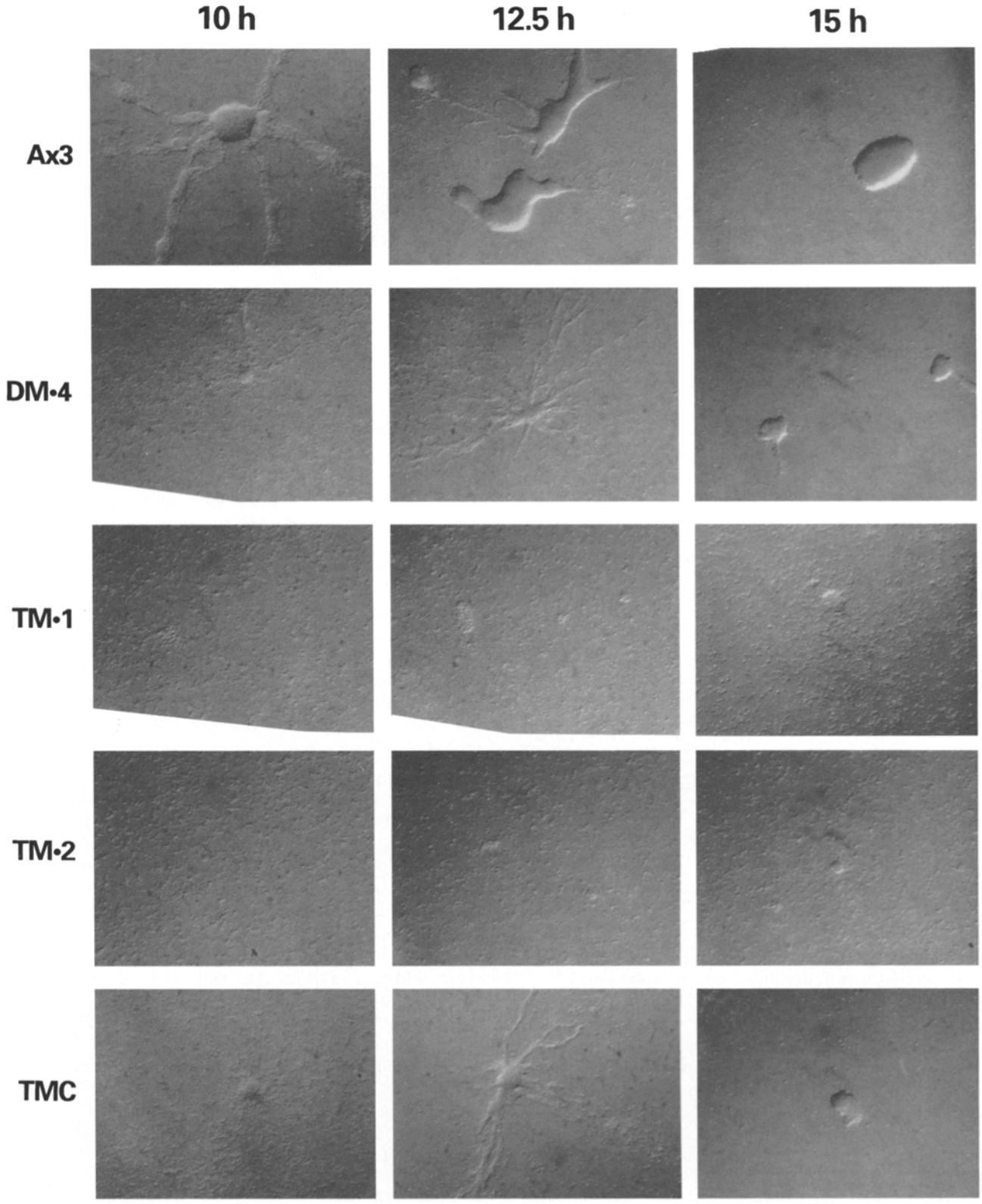

Figure 8. Streaming behavior. The indicated strains were forced to undergo chemotactic streaming as described in Materials and Methods and photographed at 10, 12.5, and 15 h using a stereo microscope (ZMU; Nikon Inc., Garden City, NY).

sively that this plateau is due to the achievement of a steady state wherein the rates of marker uptake and efflux from the cell become equal (22, 32, 41). The rate of accumulation of the marker, which is always the balance between the rate of uptake and the rate of efflux, does indeed provide the true rate of uptake for times less than 60 min because there is no appreciable efflux component over at least the first ~60 min (unlike vertebrate cells, *Dic-*

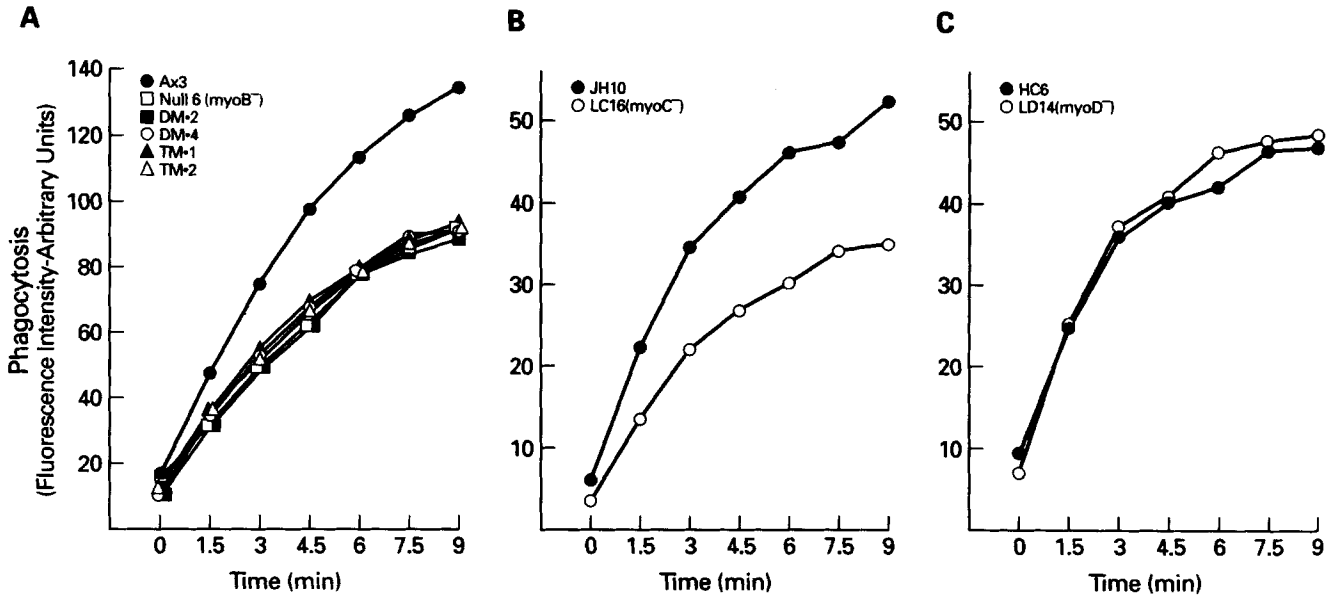

Figure 9. Phagocytosis. Shown are the initial rates of uptake of 1-μm FITC-labeled latex beads in shaking suspension culture for Ax3 cells and the mutants derived from it (*A*), as well as for representative myoC⁻ (*B*) and myoD⁻ (*C*) single mutants, together with their parental cell lines. Because these rates are not absolutely linear, the percent inhibitions reported in the text were obtained by averaging the rate differences between mutant and parental cells for each of the six 1.5-min time intervals determined. We attribute the small but significant amounts of cell-associated beads in the time 0 samples to the time interval (~20 s) between when beads were added and mixed and when the first sample (i.e., time 0) was withdrawn. As a point of reference, the fluorescence intensity value for Ax3 at 3 min corresponds to ~24 beads per cell.

tyostelium do not have an early efflux component) (22, 41, and see below).

With regard to the three single mutants, the results in Fig. 10, *A–C*, indicate that their rates of pinocytosis were slowed only slightly. Specifically, the rates exhibited by myoB⁻, myoC⁻, and myoD⁻ cells were reduced by only ~11, ~11, and ~3%, respectively, relative to their parental controls (Table III, *third column*; calculated from 30 and 60 min accumulation values in Fig. 10). These small decreases are consistent with the essentially normal doubling times of the single mutants.

In contrast to the single mutants, double mutant strains DM·2 and DM·4 exhibited more substantial reductions in pinocytic rate (Fig. 10 *A*). Specifically, the rates for DM·2 and DM·4 were reduced relative to Ax3 cells by ~39 and ~39%, respectively (Table III, *third colum*). These larger reductions are consistent with their significantly longer doubling times (Table II). Furthermore, the ~39% reduction exhibited by DM strains is ~2.8 times larger than the sum of the reductions seen in myoD⁻ (~3%) and myoB⁻ cells (~11%), indicating that a large degree of synergism occurs when a single cell lacks both of these isoforms.

The rate of pinocytosis was reduced even more in triple mutant strains (Fig. 10 *A*). Specifically, the rates for TM·1 and TM·2 were reduced by ~59 and ~60%, respectively, relative to Ax3 (Table III, *third column*). Measurements of pinocytosed volumes over a very short time course (<30 min) yielded very similar results (data not shown). The additional reduction in pinocytic rate exhibited by TM strains was due to suppression of myoC levels in a DM background because TM·C pinocytosed at a rate that was indistinguishable from that of DM·2 and DM·4 (Fig. 10 *A* and Table III, *third column*). The larger reduction in pinocytic rate observed for TM cells relative to DM cells is also consistent with measurements of doubling times (Table II), in that TM strains (but not TM·C) were ~23% slower than DM strains. Finally, the additional ~20% decrease in pinocytic rate observed in going from a double mutant to a triple mutant is about twice the size expected from the effect seen in the myoC⁻ single mutant (~11%), indicating that some degree of synergism occurs in going from the double mutant to the triple mutant. All of these inhibitions in pinocytosis were also observed with cells adherent to a surface, although the inhibitions were ~20% smaller (data not shown).

The plots in Fig. 10 also reveal (*a*) the time required for strains to reach steady state, which gets progressively

Table II. Doubling Times

Strain	Doubling Time*
	h
Ax3	8.0/8.5
NULL6	8.0/8.5
DM·2	10.0/10.0
DM·4	9.5/10.0
TM·1	12.0/12.5
TM·2	12.0/12.5
TM·C	10.0/10.0
JH10	10.0/10.5
LC16	10.5/10.5
HC6	11.0/11.0
LD14	11.0/11.5

*Shown are the results of two independent determinations, each rounded to the nearest half hour. The percentage differences presented in the text were based on the average of the two values.

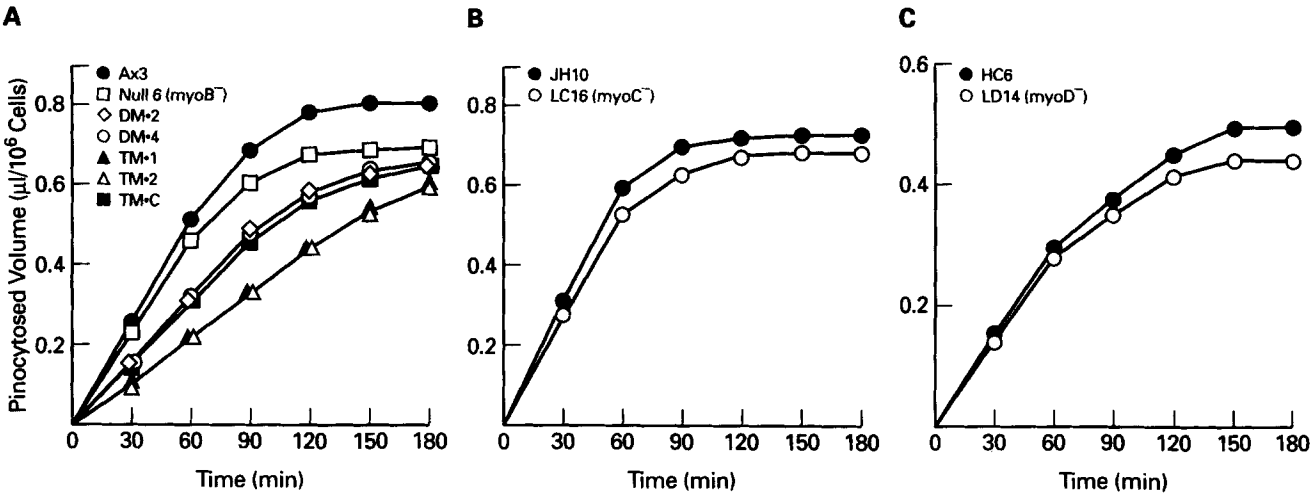

Figure 10. Kinetics of fluid phase pinocytosis (uptake). Shown is the accumulation of the fluid phase pinocytic marker FITC-dextran (converted to μl of pinocytosed media per 10^6 cells) vs. time for Ax3 cells and the mutants derived from it (*A*), as well as for representative myoC⁻ (*B*) and myoD⁻ (*C*) single mutants, together with their parental cell lines. Each value is the mean of duplicate samples. Very similar results were obtained in a second experiment and in measurements of marker accumulation over a short time course (0–30 min) (data not shown, but see Fig. 11).

longer as one goes from Ax3 (and null 6) cells, to DM-2/DM-4 cells, and then to TM-1/TM-2 cells (Table III, *fifth column*), and (*b*) the volume of the intracellular endocytic space (in μl/10^6 cells) at steady state, which is slightly smaller in several of the mutants (Table III, *sixth column*).

Double and Triple Mutants Exhibit a Corresponding Decrease in the Rate of Efflux of the Fluid Phase Pinocytic Marker Coupled with a Small Increase in Transit Time for Triple Mutants

The time required to reach steady state is influenced not only by the rate of uptake and the volume of the intracellular compartment at steady state, but also by the transit time and the efflux or egestion rate. To measure these latter two parameters, cells were incubated for 7.5 min in HL5 media containing FITC-dextran, washed free of extracellular dextran, incubated in media without the marker, and the amount of cell-associated FITC-dextran was determined at 10–15-min intervals (Fig. 11 and Table IV). The time interval between the start of the incubation without extracellular FITC-dextran (time 0 in the plots) and when the amount of cell-associated marker begins to fall represents the transit time. This is the time required for the dextran to traverse the endocytic pathway before egestion (the level of cell-associated dextran remains constant during this time because there is essentially no rapid recycling component) (22, 41). As a measure of the efflux rate, we determined the time interval between when cell-associated dextran begins to decrease and when one half

*Table III. Kinetics of Fluid Phase Pinocytosis (Uptake)**

Strain	Uptake rate	Percentage decrease in uptake rate relative to parental	Fold decrease¶ in uptake rate relative to parental	Time to steady state	Intracellular compartment size at steady state
	μl/10⁶ cell/h‡§			*min*	*μl/10⁶ cells***
Ax3	0.520	–	–	~120	0.80
NULL6	0.465	10.5	1.12×	~120	0.70
DM-2	0.315	39.4	1.65×	~180	0.65
DM-4	0.320	38.5	1.63×	~180	0.65
TM-1	0.215	58.7	2.42×	~240‖	0.65
TM-2	0.210	59.6	2.48×	~240‖	0.65
TM-C	0.310	40.4	1.68×	~180	0.65
JH10	0.590	–	–	~120	0.70
LC16	0.525	11.0	1.12×	~120	0.70
HC6	0.290	–	–	~150	0.50
LD14	0.280	3.4	1.04×	~150	0.45

*The values presented here were obtained from the data in Fig. 10.
‡Rounded to the nearest 0.005 μl.
§Based on linear regression analyses using the 30 and 60 min values in Fig. 10.
‖Based on a longer time course than that shown in Fig. 10 *A*.
¶Calculated for comparison with the fold increase in egestion half-time in Table IV.
**Rounded to the nearest 0.05 μl.

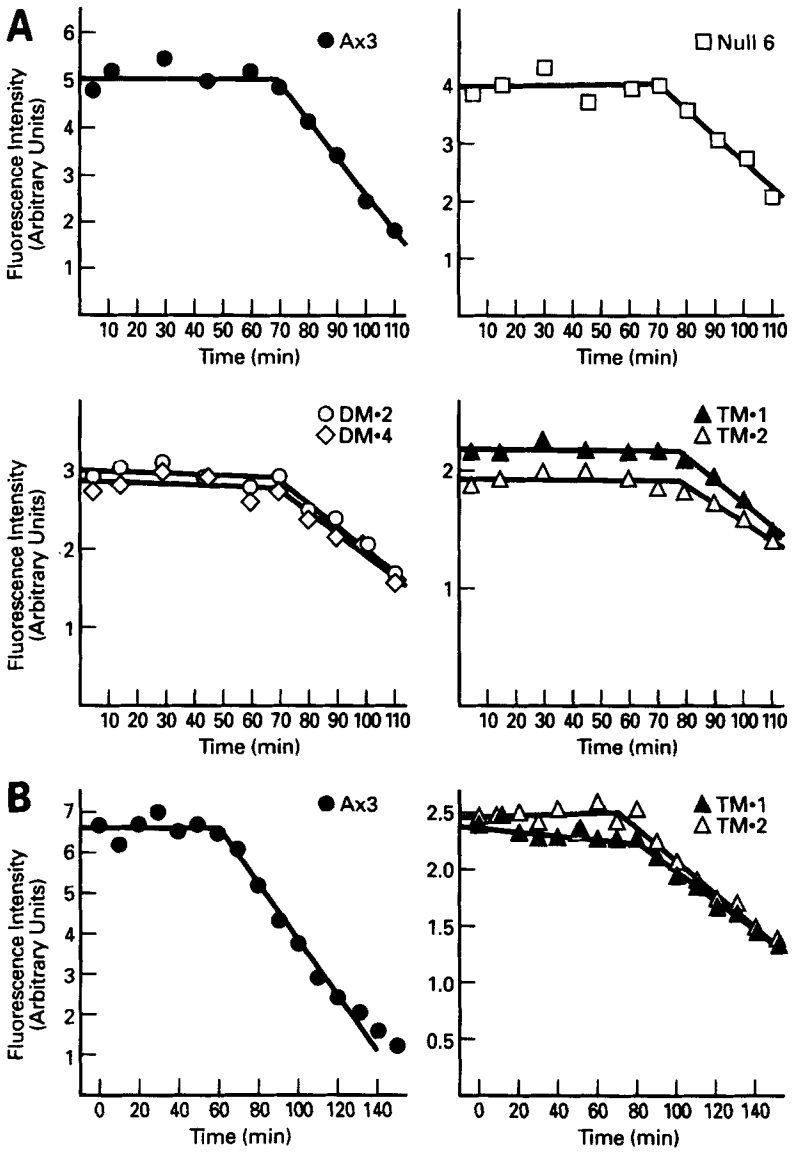

Figure 11. Kinetics of fluid phase pinocytosis (transit time and efflux). Shown is the level of cell-associated dextran vs. time after a short pulse of dextran uptake (7.5 min), followed by incubation in dextran-free media, for Ax3 cells and the mutants derived from it (*A*), and for just Ax3, TM·1, and TM·2 cells (*B*). Each value is the mean of duplicate samples. While the y-axis (whose scales are different from plot to plot) is in units of relative fluorescence, one can compare the absolute amounts of cell-associated fluorescence at time 0 (the time at which cells were resuspended in media without dextran) between the strains within experiment 1 (*A*) and between the strains within experiment 2 (*B*), because the cell concentrations were the same and because the concentration of fluorescent dextran in the media during the pulse was the same for all of the strains within each of the two experiments. Given this, note that approximately the same degree of inhibition in uptake is seen for these mutants after a 7.5-min pulse, as was obtained from the extensive accumulation data in Fig. 10 *A*. We purposely plotted the data such that the fluorescence intensities for different strains at time 0 were all approximately the same distance from the xy intercept so as to accentuate the differences in efflux rates. To obtain the slopes of the lines that span the transit time and efflux components, we used linear regression analyses on points that obviously precede and follow the break point, respectively.

of the marker is lost (the reuptake of effluxed marker is negligible because of the enormous dilution of the effluxed dextran in the media). While this value, which we refer to as egestion half-time, does not give an absolute efflux rate in $\mu l/10^6$ cells/h, it does provide a relative measure of efflux kinetics that allows the various mutant strains to be compared to control cells.

Fig. 11 *A* shows the efflux kinetics for Ax3 cells and the single, double, and triple mutants derived from it, while the calculated transit times and egestion half-times are presented in Table IV. As can be seen, there is a progressive lengthening in the egestion half-time as one goes from Ax3 cells, to null 6 cells, to DM·2 and DM·4, and then to TM·1 and TM·2 (Table IV, part *A*, *fourth column*). These changes were not accompanied by any significant changes in transit time (Table IV, part *A*, *second column*), with the possible exception of TM·1 and TM·2 cells, which exhibited transit times of ~75 and ~76 min, respectively, compared to ~68 min for Ax3 cells. The results for the TM strains were confirmed in a second experiment (Fig. 11 *B*) in which Ax3, TM·1, and TM·2 cells were analyzed over a longer time course and at more frequent time intervals. Ax3 cells exhibited a transit time of ~64 min and an egestion half-time of ~42 min, while TM·1 and TM·2 exhibited transit times of ~80 and ~70 min, respectively, and egestion half-times of ~83 and ~88 min, respectively (Table IV, part *B*, *second and fourth columns*).

The ~2.1-fold decrease in egestion half-time exhibited by TM·1/TM·2 cells (relative to Ax3), as well as the ~1.6- and ~1.3-fold decreases in egestion half-time exhibited by DM·2/DM·4 and null 6 cells, respectively, are comparable to the ~2.4-, ~1.6-, and ~1.1-fold decreases in uptake rate exhibited by these same strains, respectively (compare Table III, *fourth column* to Table IV, *fifth column*). While a true efflux rate (in $\mu l/10^6$ cells/h) was not determined here (because we cannot know the concentration of the marker at egestion), the similar decreases in egestion half-times and uptake rates suggest that the progressive decreases in uptake rate are balanced by corresponding decreases in efflux rate. The establishment of such a balance would be consistent with the fact that in axenic strains there is an enormous flux of membrane and liquid through the en-

*Table IV. Kinetics of Fluid Phase Pinocytosis (Transit time and Efflux)**

	Strain	Transit time	Time when one half of cell-associated fluorescence has been lost	Egestion half-time	Fold increase‖ in egestion half-time relative to parental (Ax3)
		min‡	min‡	min‡	
	Ax3	68	99	31	–
	NULL 6	71	112	41	1.32×
A	DM·2	68	119	51	1.64×
	DM·4	69	119	50	1.61×
	TM·1	76	136	60§	1.94×
	TM·2	75	142	67§	2.16×
	Ax3	64	106	42	–
B	TM·1	80	163	83	1.98×
	TM·2	70	158	88	2.10×

*The values presented here were obtained from the data in Fig. 11, *A* and *B*.
‡Rounded to the nearest min.
§Based on extrapolation.
‖Calculated for comparison with the fold decrease in uptake rate in Table III.

docytic pathway (1, 32, 41). Any imbalance between uptake and efflux would lead, therefore, to either rapid swelling (uptake > efflux) or shrinking (efflux > uptake) of the endocytic compartment in the cell. The efflux kinetics also show that for Ax3 cells and all the mutant strains derived from it, there was negligible efflux over the first ~60 min. The uptake rates in Table III are therefore valid. Finally, with regard to the time required to reach steady state, it seems likely that the small changes in both transit time and intracellular compartment size have little effect, such that the majority of the increases in time to steady state are due to the decreases in fluid phase endocytic flux (uptake and efflux).

Fluorescence Micrographs of Cells Labeled with Texas Red–Dextran Suggest That the Normal Process of Pinosome Maturation Is Aberrant in Triple Mutant Cells

In an effort to gain some insight into the mechanism by which endocytic flux is reduced in our mutants, Ax3 and TM cells were allowed to endocytose dextran labeled with Texas red for 15 min, rapidly washed free of extracellular dextran, and immediately photographed with the fluorescence microscope. Fig. 12 shows the typical appearance of Ax3 cells and TM·1 cells (each image contains several cells in close association). While we have not attempted to measure precisely either the number or size distribution of fluorescent vesicles, it appears that TM cells contain a significantly larger number of vesicles than do Ax3 cells, and that these vesicles are of a smaller average size than in Ax3 cells. Based on the recent experiments of Nolta et al. (29), who determined the sizes of intracellular vesicles that contain pinocytosed dextran as a function of the time after uptake, it would appear that TM cells are slower in some aspect of the maturation process for primary pinosomes (see Discussion).

Discussion

The introduction of mutations, especially multiple mutations, into a particular *Dictyostelium* cell line opens up the possibility that some phenotypic defects observed are not due in fact to the absence of the targeted gene product(s), but to secondary and unintended changes in the genome resulting from the transformation events. To address this potential problem, we analyzed independent mutant isolates and showed that they have similar phenotypes. We previously established (18, 61) that strain null 6, which we used here as the starting point for creating double and triple mutants, was indeed representative of a number of independent myoB$^-$ clonal isolates. This is also the case for the myoD$^-$ strain LD14 (21) and the myoC$^-$ strain LC16 (data not shown). For the double mutants of myoB and myoD, we have presented similar data here for two independent isolates (DM·2 and DM·4), and experiments with two other independent lines (DM·1 and DM·3) gave similar results (data not shown). For the triple mutants, we also analyzed two independent isolates in detail (TM·1 and TM·2) and obtained similar results for both. In addition, partial analysis of several other independent TM lines yielded very similar results (data not shown). Finally, we showed in a number of experiments that TM·C, a phleomycin-resistant clone with near normal levels of myoC, behaves like its most immediate parental strain, DM·4.

Motility Phenotypes

In separate experiments, we found that vegetative Ax3 cells crawl at ~25% of the rate of ripple-stage cells, and that the transition to the higher speeds exhibited by ripple-stage cells occurs over an ~90-min period immediately preceding the onset of ripple stage (data not shown). This switch in motility phenotype, which involves a large increase in the degree of cell polarization as well as in cell speed, has been reported by others (48, 58, 61) and underscores the idea that aggregation-stage cells and not vegetative cells represent the better choice for examining the effects of targeted gene disruptions on whole cell motility. Unlike a previous report (58), however, we found that the speed of Ax3 cells did not decline significantly in the 2-h period after ripple stage (during which time the cells advanced from ripple stage [~7 h] to the tight mound stage [~9 h]) (data not shown). Similarly, in two experiments null 6 and TM·1 cells exhibited mean speeds at mound stage that were not obviously different from their speeds

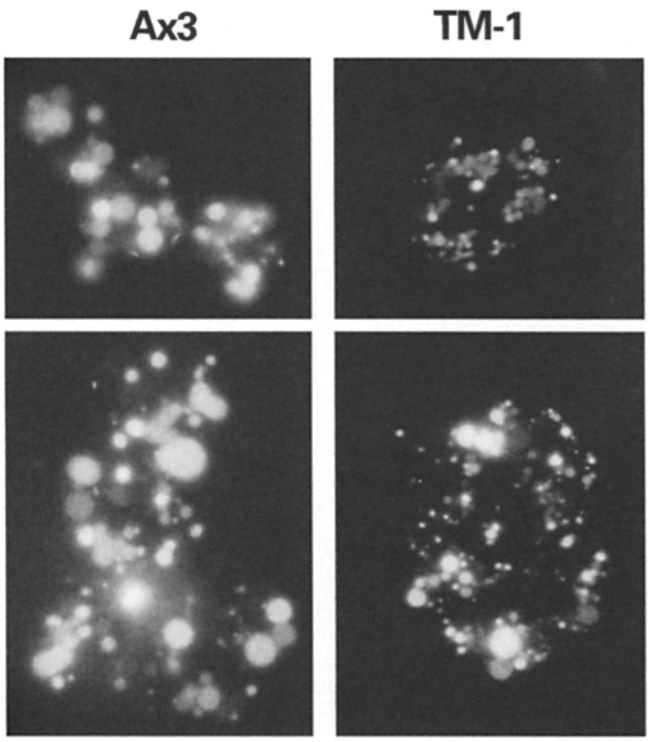

Figure 12. Fluorescent micrographs of Ax3 and TM·1 cells loaded for 15 min with Texas red–labeled dextran. Cells were allowed to pinocytose Texas red–dextran in suspension culture for 15 min, rapidly separated from uningested dextran, and immediately photographed. Shown are two separate examples for each strain. The upper and lower images of Ax3 cells have three and four cells in close association, respectively, while the upper and lower images of TM·1 cells have two and three cells in close association, respectively. It is important to note that these photographs represent just a single (and presumably representative) focal plane through these cells, so they actually contain many more dextran-containing vesicles per cell than can be counted in these images (see also reference 29). The actual fluorescent intensities of labeled vesicles in TM·1 cells were considerably fainter relative to Ax3 cells than shown here (due presumably to the reduced amount of dextran taken up by TM cells). This difference was sacrificed to produce prints in which the size and number of labeled vesicles in TM·1 cells were more obvious.

at ripple stage (data not shown). It seems unlikely, therefore, that (*a*) the slower speeds recorded for our mutants are due to a systematic error on our part in the somewhat qualitative judgement as to what constitutes ripple stage, and (*b*) that the slower speeds at ripple stage are simply the result of an overall delay in the onset of the phenotypic switch mentioned above (assuming that it can be uncoupled from the morphological signpost of ripple stage).

Of the three single mutants, only myoB$^-$ cells were significantly slower than control cells. MyoB$^-$ cells were also the only single mutants to be significantly impaired in streaming behavior. These facts, together with the fact that the protein level of myoB alone was dramatically elevated relative to vegetative cell level in aggregation-stage cells, are consistent with the idea that of these three isoforms, myoB has the dominant role in whole cell motility (as defined by our assay). We also found, however, that the concentration of myoB is much higher than that of both myoC and myoD in ripple-stage cells. One might expect, therefore, that the absence of myoC and myoD would have a much smaller effect than the absence of myoB if the relative contributions of the individual isoforms to whole cell motility are directly proportional to their concentrations in the cell. Indeed, myoC and myoD may contribute even more to whole cell motility than myoB on a per molecule basis. We cannot exclude the possibility, therefore, that myoB, myoC, and myoD may perform very similar roles in whole cell motility, despite the data reported in Table I (which would be consistent with their colocalizations at the leading edge of migrating cells). One must be careful in extending these arguments too far, however, since intracellular concentration and functional significance need not correlate. For example, only a fraction of the total number of molecules of each isoform are probably involved in any particular process under study. One apparent example of this is the reported role of *Acanthamoeba* myosin IC in the contraction of the contractile vacuole (9), which has been ascribed to the ~1% of cellular myosin IC that is on this membrane (2). For the myosins I, the ratio of phosphorylated (active) to unphosphorylated (inactive, but still able to cross-link actin) molecules is another critical (and unknown) variable (3).

MyoC and myoD (and even myoB) may also contribute to aspects of cell movement other than whole cell motility as we have assayed it (e.g., movements in the Z axis, orientation in a chemotactic gradient, and generation of traction force). Indeed, the strong effect that the absence of myoC has on streaming behavior (in a DM background) suggests that it plays an important role in some aspect of cell motility which, while not evident in our motility measurements, is evident when a large number of cells are undergoing chemotactic aggregation. The measurements of a broader range of motility parameters may uncover this role.

The final challenge will be to determine at the molecular level what role these isoforms perform in supporting cell motility and streaming behavior. As described by Condeelis (5), the contractile tension that these classic myosin I isoforms may generate within cortical actin meshworks could cause forward locomotion, retrograde actin flow, and pseudopod retraction. One might expect, therefore, to see defects in the temporal and spatial dynamics of pseudopods, in the 3D organization of the actin meshworks within them, and in the mechanical properties of the cortical actin cytoskeleton. These aspects of cytoskeletal structure and function could be examined by a combination of quantitative video microscopy[4] (48), electron microscopy (6,16), and biophysical studies (33).

Phagocytosis Phenotypes

As in a previous report (59), we found that the rate of uptake of nondigestible latex beads was approximately linear for only ~10 min. In extended time courses (10–30 min; data not shown), all of the strains exhibited a second

4. We did not present an analysis of pseudopod extension/retraction using the commonly used differencing method (48) (despite already having all of the raw data to do this in the DIAS files), because we find this method difficult to interpret when control and experimental cells exhibit significantly different speeds.

slower phase of bead accumulation (~20% of the rate from 0 to 5 min). This slower phase was not due to the achievement of a partial steady state, but to a true reduction in the rate of uptake, since cells fed beads for 2.5 min and then incubated in media without beads showed no significant loss of internalized beads for 30 min (data not shown). This lack of a significant early efflux component indicates that the rates of accumulation in Fig. 9 do indeed equal the rates of uptake and precludes the possibility that the rate of uptake by TM cells is actually slower than that of myoB$^-$ or myoC$^-$ cells, with the slower rate masked by a decrease in the efflux rate.

The fact that significant reductions in the rate of phagocytosis were observed in single mutants of myoB and myoC indicates that these two isoforms do not compensate for each other, which in turn implies that they perform distinct (or at least not fully redundant) roles in supporting the phagocytic process. The assignment of functions as either shared or distinct may depend, therefore, on whether one is considering the efficiency of a complex cellular process as a whole (in which case myoB and myoC could be said to have shared functions), or some particular step within that process (in which case they would be said to probably have distinct functions). In either case, it is clear that neither isoform is required for the phagocytic process to occur, but only for it to occur efficiently. Whatever their functions are, they are not additive in TM cells. While this result is somewhat surprising, it does support the idea that those cellular functions that are more impaired in TM cells than in DM cells (e.g., endocytosis and streaming) are not so because of some overall diminution in the "health" of TM cells.

Phagocytosis is an inducible process that is known to be actin-dependent (4, 51). Therefore, myoB and myoC could contribute to the mechanical aspects of particle engulfment in much the same way as they have been proposed to contribute to cell locomotion (5). MyoB has been localized by immunofluorescence to phagocytic cups (10), but the localization of myoC remains to be determined. In any case, localizations at the EM level may be required to discern any subtle differences that might underlie the facts that their functions are both nonredundant and not additive.

Endocytosis Phenotypes

While the sum of the inhibitions in fluid phase pinocytic rate exhibited by the three single mutants was ~25%, triple mutant cells exhibited an inhibition of ~60%. Therefore, not only do all three isoforms share in supporting the endocytic process, but the sum of their contributions is more than additive. This synergism was most striking when myoD levels were suppressed in myoB$^-$ cells, but was also evident when myoC levels were suppressed in DM cells.

In many cell types, the rate of fluid uptake can be largely if not totally accounted for by clathrin-dependent, receptor-mediated endocytosis (40, 46). This also appears to be the case in *Dictyostelium* because clathrin-deficient cells accumulate fluid phase markers at ~12% the rate of wild-type cells (31) (and this defect is not due to an acceleration in the efflux rate [44]). What is the role, then, of the actin-based motor myosin I in this type of pinocytosis, where pinosome formation is thought to be driven by clathrin coat formation coupled with dynamin function? A number of groups have reported that cytochalasins, which depolymerize F-actin, inhibit receptor-mediated endocytosis (for review see 40, 46). For example, Gottlieb et al. (11) recently showed that the actin cytoskeleton plays a role in both fluid phase and receptor-mediated endocytosis at the apical surface of polarized epithelial cells. Furthermore, both actin and fimbrin are required in yeast for receptor-mediated endocytosis (24). These results suggest that the correct functioning of the cortical actin cytoskeleton is required for efficient formation of the small (~0.1-μm-diam) coated pinosomes characteristic of clathrin-dependent endocytosis. To the extent that this is the case in *Dictyostelium*, these three myosins I could play a significant role in the endocytic process.

Dictyostelium might also possess a significant clathrin-independent (possibly actomyosin I–dependent) endocytic pathway. Evidence is growing for such a pathway in vertebrate cells (7, 14, 40, 46). For example, 3T3 fibroblasts in which clathrin polymerization has been completely blocked exhibit no significant decrease in either fluid phase or receptor-mediated endocytosis (7). An analysis of nascent pinosome size and characteristics indicated that endocytosis persisted in these cells via the formation of small uncoated vesicles whose size (~0.1 μm) was indistinguishable from that of typical coated vesicles. While the simplest interpretation of the clathrin mutant data would appear to rule out the existence of such a pathway in *Dictyostelium*, there are alternative explanations. For example, a significant portion of the uptake defect in such mutants may be secondary to primary defects in the secretory pathway (which involves coated vesicles and which is defective in clathrin mutants [31, 44]). Such an indirect effect would be similar to the strong block in fluid phase endocytosis exhibited by many yeast *sec* mutants (39). Alternatively, the pinocytic defect may be a secondary consequence of the demonstrated defects in contractile vacuole function that clathrin mutants (31) exhibit (especially if the contractile vacuole plays a significant role in the normal expulsion of water brought into the cell via pinocytosis). The formation of the small uncoated pinosomes in this clathrin-independent pathway could be even more dependent on cortical actomyosin I activity than in the clathrin-dependent pathway.

In addition to the micropinocytic processes that involve small coated and uncoated vesicles, some cells exhibit a form of fluid phase endocytosis referred to as macropinocytosis (for review see 52, 60). This type of endocytosis, which has been documented in several vertebrate cell types, accompanies cell surface ruffling. While it may occur constitutively at a low level in some cells, it is primarily an induced phenomenon that is significant only when ruffling activity is dramatically elevated by agents such as growth factors and phorbol esters (37). As the name implies, nascent macropinosomes are large, averaging ~1–1.5 μm in diam (15). Their size appears to be dictated by their mechanism of formation, wherein membrane ruffles close back on the plasma membrane, capturing extracellular fluid and resulting in the formation of large coatless pinosomes. The large, broad ruffles seen in stimulated cells often form macropinosomes, while the small ruffles characteristic of unstimulated cells usually do not (15). Be-

cause the formation of macropinosomes is dependent on membrane ruffling, which in turn is dependent on the dynamics of cortical F-actin, it is not difficult to imagine a variety of mechanistic roles for myosins I in this process. We note, however, that while macropinocytosis may occur in *Dictyostelium*, for axenic strains grown in suspension, it is probably at best only a very minor component of total fluid uptake, since the vast majority of fluid uptake under these conditions can be accounted for in small pinosomes (~0.1–0.2 μm in diam after a 3-min pulse of marker [29], which is much more consistent with the size of coated and uncoated micropinosomes). While it is possible that *Dictyostelium* macropinosomes are on average much smaller than their counterparts in vertebrate cells, the mechanism of macropinosome formation would argue against this. It seems unlikely, therefore, that the endocytic defects observed here are due to inhibition of macropinocytosis.

Recent studies by Nolta et al. (29) suggest that the endocytic pathway in *Dictyostelium* can be viewed largely as a linear, multistep process (e.g., primary pinosome formation, fusion of temporal cohorts, fusion with preexisting endocytic vesicles, maturation through the digestive pathway, and efflux). Because the flux of membrane and liquid through this pathway is so enormous (22, 32, 41), it seems likely that the rates of the individual steps are controlled and that they are all set to approximately the same rate. If such a balance was not maintained, the various endocytic compartments could at any time rapidly swell or shrink, leading to severe problems in cell viability. In such a system, if one generates a mutation that significantly impairs a step anywhere in the pathway, all of the other steps in the pathway would need to be downregulated to the new slower rate (this downregulation could be rapid, resulting from feedback controls that respond quickly, or may manifest itself only in the long selection process used to obtain viable transformants). So the point at which the myosin I mutations/antisense suppressions described here act to inhibit pinocytic flux could be quite distant from the actual formation of nascent pinosomes at the plasma membrane, yet still result in the observed reductions in uptake rate. For example, the absence of myosin I may impair the movement of formed pinosomes or the membrane movements involved in endosome maturation. The ability of these classic myosins I to bind to membranes (12, 23, 28, 36), and the localization of *Acanthamoeba* myosins I to endocytic vacuoles (2, 3), are both consistent with such a role, although the skeletal muscle myosin-like duty cycle exhibited by *Acanthamoeba* myosins IA and IB (Ostap, E.M., and T.D. Pollard. 1995. *Biophys. J.* 8:159*a*) puts important constraints on the roles of these molecules as vesicle motors. The absence of these isoforms could also impair contractile vacuole function, resulting in a reduction in the ability of the cell to handle the large volume of water brought in by endocytosis and leading to a compensatory decrease in the rate of fluid uptake. This scenario is particularly interesting because a myosin I in *Acanthamoeba* has been implicated in contractile vacuole function (9). We note, however, that we have not observed staining of the contractile vacuole complex with our isoform-specific antibodies to myoB, myoC, and myoD, and TM cells are not hypersensitive to hypotonic media (data not shown).

Defects in fluid-phase pinocytosis resulting from myosin I knockouts have also been reported recently by Novak et al. (30), who observed no apparent reduction in myoA$^-$, myoB$^-$, and myoC$^-$ single mutants but significant reductions in myoA$^-$/myoB$^-$ and myoB$^-$/myoC$^-$ double mutants grown in suspension. Like our data, their results are consistent with the idea that multiple myosin I isoforms share in supporting the endocytic process, although in contrast to our experiments their mutant collection substituted one of the truncated isoforms (myoA) for one of the classic isoforms (myoD). Unlike our study, those authors found that (*a*) the inhibition completely disappeared when pinocytosis was measured using double mutant cells that were adherent to a surface, and (*b*) that double mutants growing in suspension exhibited very long doubling times and entered stationary phase at very low cell densities.

Photographs of wild-type and TM cells labeled for 15 min with Texas red–conjugated dextran suggest an apparent shift in TM cells towards (*a*) a larger number of fluorescent vesicles and (*b*) a smaller average size. Using a magnetic technique to purify intracellular vesicles containing endocytosed ferritin-dextran at various times after uptake, Nolta et al. (29) have shown that nascent ~0.1-μm-diam pinosomes fuse together and with preexisting endocytic vesicles so that by 15 min the average diameter of intracellular vesicles containing the marker is ~0.5–0.75 μm. Our results using Texas red–dextran suggest, therefore, that TM cells are slower in some aspect of this maturation process. The application to our mutants of this magnetic technique should provide a quantitative yard stick to the largely qualitative data in Fig. 10.

Finally, with regard to the correlation between the inhibition in pinocytic flux and the lengthening of division times, while we cannot prove a cause–effect relationship, we note that (*a*) all of the many independent TM lines that expressed very low levels of myoC protein also demonstrated slow growth rates, and (*b*) some TM lines that reverted relatively rapidly in terms of myoC protein levels also reverted simultaneously in terms of growth rate (to DM rates).

Summary

Two genes are functionally redundant if each can partially or fully substitute for the other. Recently, Thomas (53) described several mechanisms by which redundant genes can be stably maintained. For example, two genes that have shared (i.e., overlapping) functions can be maintained through selection for an additional function(s) that is unique to each gene. Even if one considers only the clear cut cases, this type of partial redundancy appears to be quite common (53). We began the work described in this paper with the knowledge that while myoB$^-$ single mutants exhibit scorable phenotypes, the defects are not extremely striking (19, 61). Furthermore, initial analyses of myoC$^-$ (34) and myoD$^-$ (21) single mutants did not reveal any obvious defects (these results contrast with the knockout of an *Aspergillus* myosin I, which is lethal [27]). Given the strong similarities between these three classic myosin I isoforms in terms of their tail domain sequences (and biochemistry) and their colocalization within actin-rich cortical regions in migrating cells, we thought that the weak phenotypes exhibited by the single mutants (especially

myoC$^-$ and myoD$^-$ cells) were most likely due to functional compensation by the remaining two classic myosin I isoforms.[5] If such compensation were occurring, it should be evident in cells that lack two or more of these myosins as additive/synergistic defects in those cellular processes supported by these motors. To address this question, we analyzed the behaviors of single, double, and triple mutants of myoB, myoC, and myoD.

The data that we obtained, when taken together, clearly excludes the extreme case that all three of these classic myosin I isoforms perform exclusively the same functions. For example, (*a*) both the motility data and the protein expression data indicate that myoB alone plays a significant role in the whole cell motility of aggregation-stage cells, (*b*) only two of the three isoforms play roles in the process of phagocytosis, and their roles appear to be nonredundant, and (*c*) myoC appears to support streaming behavior through a mechanism that is distinct from that for myoB. This evidence of functional specialization is consistent with the subset of unique localizations seen for three classic myosin I isoforms from *Acanthamoeba* at the EM level (2, 3), and with the fact that the absence of *Dictyostelium* myoB is not fully compensated for in myoB$^-$ cells (19, 61).

We did find one cellular process, however, that was supported to a significant extent by all three isoforms. Not only do all three share in supporting the process of fluid phase endocytosis, but the sum of their contributions is more than additive. It is important to stress, however, that endocytosis is a complex, multistep process, and that at this point we do not know whether these three isoforms support the efficiency of the same step (which works best when all three isoforms are present and progressively worse as each is eliminated), or whether they support the efficiency of different steps within the endocytic process. In the former case, these three proteins could be said to have truly overlapping roles, while in the latter case they could be said to have nonoverlapping roles in supporting the same complex cellular process. To resolve this question, we need to understand the endocytic process in much greater detail and to identify the step(s) in this process where these myosins function.

Finally, our data underscored two significant complications with regard to inferring functions from mutant phenotypes. The first is that when one analyzes cells carrying multiple mutations in closely related protein isoforms, significant differences in the absolute amounts of these isoforms must be factored into conclusions regarding the possibility of functional overlap. This complication applied principally to our motility data. The second complication is that the assignment of functions as overlapping or nonoverlapping may depend on whether one is considering a complex, multistep cellular process as a whole, or some particular step in that process. This complication applies to those situations where one's assay is simply measuring the efficiency of an entire complex cellular process. This point may be relevant to the results obtained with a single mutant in one of the truncated myosin I isoforms (myoA), which, like myoB$^-$ cells, exhibits a slower rate of whole cell locomotion (55) and, when combined with the absence of one of the classic myosin I isoforms (myoB), contributes to an inhibition in endocytic flux (30). These results imply either that the striking differences in tail domain structure between classic and truncated myosin I isoforms are not functionally significant, or that these two apparent subfamilies contribute to supporting the same complex cellular processes but at different steps in these processes. We favor the latter hypothesis.

5. We note that Southern blot analyses (13, 21), together with the recent analysis of a *Dictyostelium* YAC library (56), indicate that this organism contains 10–13 actin-based motor proteins, seven of which have been fully sequenced (8, 13, 20, 21, 34, 54, 57). All or some of the remaining three to six putative myosin genes could encode type I myosins, further complicating the situation.

We thank Drs. Edward D. Korn and Ted Steck for their helpful comments, and Dr. Ivan Baines for discussions regarding endocytic flux.

Received for publication 8 November 1995 and in revised form 1 February 1996.

References

1. Bacon, R.A., C.J. Cohen, D.A. Lewin, and I. Mellman. 1994. *Dictyostelium discoideum* mutants with temperature-sensitive defects in endocytosis. *J. Cell Biol.* 127:387–399.
2. Baines, I.C., H. Brzeska, and E.D. Korn. 1992. Differential localization of *Acanthamoeba* myosin I isoforms. *J. Cell Biol.* 119:1193–1203.
3. Baines, I.C., A. Corigliano-Murphy, and E.D. Korn. 1995. Quantification and localization of phosphroylated myosin I isoforms in *Acanthamoeba castellanii*. *J. Cell Biol.* 130:591–603.
4. Cohen, C.J., R. Bacon, M. Clarke, K. Joines, and I. Mellman. 1994. *Dictyostelium discoideum* mutants with conditional defects in phagocytosis. *J. Cell Biol.* 126:955–966.
5. Condeelis, J. 1993. Understanding the cortex of cawling cells: insights from *Dictyostelium*. *Trends Cell Biol.* 3:371–376.
6. Cox, D., J.A. Ridsdale, J. Condeelis, and J. Hartwig. 1994. Genetic deletion of ABP-120 alters the three-dimensional organization of actin filaments in *Dictyostelium* pseudopods. *J. Cell Biol.* 128:819–835.
7. Cupers, P., A. Viethen, A. Kiss, P. Bavdhiun, and P.S. Courtoy. 1994. Clathrin polymerization is not required for bulk-phase endocytosis in rat fetal fibroblasts. *J. Cell Biol.* 127:725–735.
8. DeLozanne, A., and J.A. Spudich. 1987. Disruption of the *Dictyostelium* myosin heavy chain gene by homologous recombination. *Science (Wash. DC).* 236:1080–1091.
9. Doberstein, S.K., I.C. Baines, G. Wiegand, E.D. Korn, and T.D. Pollard. 1993. Inhibition of contractile vacuole function *in vivo* by antibodies against myosin-I. *Nature (Lond.).* 356:841–843.
10. Fukui, Y., T.J. Lynch, H. Brzeska, and E.D. Korn. 1989. Myosin I is located at the leading edges of locomoting *Dictyostelium* amoebae. *Nature (Lond.).* 341:328–331.
11. Gottlieb, T.A., I.E. Ivanov, M. Adesnik, and D.D. Sabatini. 1993. Actin microfilaments play a critical role in endocytosis at the apical but not the basolateral surface of polarized epithelial cells. *J. Cell Biol.* 120:695–710.
12. Hammer, J.A., III. 1994. The structure and function of unconventional myosins: a review. *J. Muscle Res. Cell Motil.* 15:1–10.
13. Hammer, J.A., III, and G. Jung. 1996. The sequence of the *Dictyostelium myoJ* heavy chain gene predicts a novel, dimeric, unconventional myosin with a heavy chain molecular mass of 258 kDa. *J. Biol. Chem.* 271:7120–7127.
14. Hansen, S.H., K. Sandvig, and B. van Deurs. 1993. Molecules internalized by clathrin-independent endocytosis are delivered to endosomes containing transferrin receptors. *J. Cell Biol.* 123:89–97.
15. Hewlett, L.J., A.R. Prescott, and C. Watts. 1994. The coated pit and macropinocytic pathways serve distinct endosome populations. *J. Cell Biol.* 124: 689–703.
16. Hug, C., P.Y. Jay, I. Reddy, J.G. McNally, P.C. Bridgeman, E.L. Elson, and J.A. Cooper. 1995. Capping protein levels influence actin assembly and cell motility in *Dictyostelium*. *Cell.* 81:591–600.
17. Janmey, P.A. 1991. Mechanical properties of cytoskeletal polymers. *Curr. Opin. Cell Biol.* 2:4–11.
18. Jung, G., and J.A. Hammer III. 1990. Generation and characterization of *Dictyostelium* cells deficient in a myosin I heavy chain isoform. *J. Cell Biol.* 110:1955–1964.
19. Jung, G., and J.A. Hammer III. 1994. The actin binding site in the tail domain of *Dictyostelium* myosin IC (myoC) resides within the glycine- and proline-rich sequence (tail homology region 2). *FEBS Lett.* 342:197–201.
20. Jung, G., C.L. Saxe III, A.R. Kimmel, and J.A. Hammer III. 1989. *Dictyostelium discoideum* contains a gene encoding a myosin I heavy chain. *Proc. Natl. Acad. Sci. USA.* 86:6186–6190.
21. Jung, G., Y. Fukui, B. Martin, and J.A. Hammer III. 1993. Sequence, ex-

pression pattern, intracellular localization and targeted disruption of the *Dictyostelium* myosin-ID heavy chain isoform. *J. Biol. Chem.* 268:14981–14990.

22. Klein, G., and M. Satre. 1986. Kinetics of fluid phase pinocytosis in *Dictyostelium discoideum* amoebae. *Biochem. Biophys. Res. Commun.* 138: 1140–1152.
23. Korn, E.D., M.A.L. Atkinson, H. Brzeska, J.A. Hammer III, G. Jung, and T.J. Lynch. 1988. Structure-function studies of *Acanthamoeba* myosins IA, IB, and II. *J. Cell. Biochem.* 36:37–50.
24. Kubler, E., and H. Riezman. 1983. Actin and fimbrin are required for the internalization step of endocytosis in yeast. *EMBO (Eur. Mol. Biol. Organ.) J.* 12:2855–2862.
25. Laemmli, U.K. 1970. Cleavage of structural proteins during assembly of the head of bacteriophage T4. *Nature (Lond.).* 227:680–685.
26. Lee, S., and G.P. Côte. 1993. Isolation and characterization of three *Dictyostelium* myosin-I isozymes. *J. Biol. Chem.* 268:20923–20929.
27. McGoldrick, C.A., C. Gruver, and G.S. May. 1995. *myoA* of *Aspergillus nidulans* encodes an essential myosin I required for secretion and polarized growth. *J. Cell Biol.* 128:577–587.
28. Mooseker, M.S., and R.E. Cheney. 1995. Unconventional myosins. *Annu. Rev. Cell Develop. Biol.* 11:633–675.
29. Nolta, K.V., J.M. Rodriguez-Paris, and T.L. Steck. 1994. Analysis of successive endocytic compartments isolated from *Dictyostelium discoideum* by magnetic fractionation. *Biochem. Biophys. Acta.* 1224:237–246.
30. Novak, K.D., M.D. Peterson, M.C. Reedy, and M.A. Titus. 1995. *Dictyostelium* myosin I double mutants exhibit conditional defects in pinocytosis. *J. Cell Biol.* 131:1205–1221.
31. O'Halloran, T.J., and R.G. Anderson. 1992. Clathrin heavy chain is required for pinocytosis, the presence of large vacuoles, and development in *Dictyostelium*. *J. Cell Biol.* 118:1371–1377.
32. Padh, H., J. Ha, M. Lavasa, and T.L. Steck. 1993. A post-lysosomal compartment in *Dictyostelium discoideum*. *J. Biol. Chem.* 268:6742–6747.
33. Pasternak, C.J., J.A. Spudich, and E. Elson. 1989. Capping of surface receptor and concomitant cortical tension are generated by conventional myosin. *Nature (Lond.).* 341:549–551.
34. Peterson, M.D., K.D. Novak, M.C. Reedy, J.I. Ruman, and M.A. Titus. 1995. Molecular genetic analysis of myoC, a *Dictyostelium* myosin I. *J. Cell Sci.* 108:1093–1103.
35. Podolski, J.L., and T.L. Steck. 1990. Length distribution of F-actin in *Dictyostelium discoideum*. *J. Biol. Chem.* 265:1312–1318.
36. Pollard, T.D., S.K. Doberstein, and H.G. Zot. 1991. Myosin-I. *Annu. Rev. Physiol.* 53:653–681.
37. Racoosin, E.L., and J.A. Swanson. 1992. M-CSF-induced macropinocytosis increases solute endocytosis but not receptor-mediated endocytosis in mouse macrophages. *J. Cell Sci.* 102:867–880.
38. Reinhard, J., A.A. Scheel, D. Diekman, A. Hall, C. Ruppert, and M. Bahler. 1995. A novel type of myosin implicated in signalling by rho family GTPases. *EMBO (Eur. Mol. Biol. Organ.) J.* 14:697–704.
39. Riezman, H. 1985. Endocytosis in yeast: several of the yeast secretory mutants are defective in endocytosis. *Cell.* 40:1001–1009.
40. Riezman, H. 1993. Three clathrin-dependent budding steps and cell polarity. *Trends Cell Biol.* 3:330–332.
41. Rodriquez-Paris, J.M., and K.V. Nolta, and T.L. Steck. 1993. Characterization of lysosomes isolated from *Dictyostelium discoideum* by magnetic fractionation. *J. Biol. Chem.* 268:9110–9116.
42. Rosenfeld, S.S., and B. Rener. 1994. The GPQ-rich segment of *Dictyostelium* myosin IB contains an actin binding site. *Biochemistry.* 33:2322-2328.
43. Rubino, S., and J.V. Small. 1987. The cytoskeleton of spreading *Dictyostelium* amoebae. *Protoplasma.* 136:63–69.
44. Ruscetti, T., J.A. Cardelli, M.L. Niswonger, and T.J. O'Halloran. 1994. Clathrin heavy chain functions in sorting and secretion of lysosomal enzymes in *Dictyostelium discoideum*. *J. Cell Biol.* 126:343–352.
45. Sambrook, J., F. Fritsch, and T.E. Maniatis. 1989. Molecular Cloning: A Laboratory Manual. Cold Spring Harbor Laboratory, Cold Spring Harbor, New York. 545 pp.
46. Sandvig, K., and B. van Deurs. 1994. Endocytosis without clathrin. *Trends Cell Biol.* 4:275–277.
47. Solc, C.K., R.H. Derfler, G.M. Duyk, and D.P. Corey. 1994. Molecular cloning of myosins from bullfrog saccular maculla: a candidate for the hair cell adaption motor. *Auditory Neurosci.* 1:63–75.
48. Soll, D.R., E. Voss, B. Varnum-Finney, and D. Wessels. 1988. The dynamic morphology system: a method for quantitating changes in shape, pseudopod formation and motion in normal and mutant amoebae of *Dictyostelium discoideum*. *J. Cell. Biochem.* 37:177–192.
49. Spudich, J.A., editor. 1987. *Dictyostelium discoideum*: molecular approaches to cell biology. *In* Methods in Cell Biology. Vol. 28. Academic Press, New York. 516 pp.
50. Stoller, H., C. Ruppert, J. Reinhard, and M. Bahler. 1995. A novel mammalian myosin I from rat with an SH3 domain localizes to Con A inducible, F-actin–rich structures at cell–cell contacts. *J. Cell Biol.* 129:819–830.
51. Swanson, J.A., and S.C. Baer. 1995. Phagocytosis by zippers and triggers. *Trends Cell Biol.* 5:89–93.
52. Swanson, J.A., and C. Watts. 1995. Macropinocytosis. *Trends Cell Biol.* 5: 424–428.
53. Thomas, J.H. 1993. Thinking about genetic redundancy. *Trends Genet.* 9: 395–399.
54. Titus, M.A., H.M. Warrick, and J.A. Spudich. 1989. Multiple actin-based motor genes in *Dictyostelium*. *Cell Regul.* 1:55–63.
55. Titus, M.A., D. Wessels, J.A. Spudich, and D. Soll. 1993. The unconventional myosin encoded by the *myo A* gene plays a role in *Dictyostelium* motility. *Mol. Cell. Biol.* 4:233–246.
56. Titus, M.A., A. Kuspa, and W.F. Loomis. 1994. Discovery of myosin genes by physical mapping in *Dictyostelium*. *Proc. Natl. Acad. Sci. USA.* 91: 9446–9450.
57. Urrutia, R.A., G. Jung, and J.A. Hammer III. 1993. The *Dictyostelium* myosin IE heavy chain gene encodes a truncated isoform that lacks sequences corresponding to the actin binding site in the tail. *Biochem. Biophys. Acta.* 1173:225–229.
58. Varnum, B., K. Edwards, and D.R. Soll. 1985. The developmental regulation of single cell motility in *Dictyostelium discoideum*. *Dev. Biol.* 113: 218–227.
59. Vogel, G., L. Thilo, H. Schwarz, and R. Steinhart. 1980. Mechanism of phagocytosis is mediated by different recognition sites as disclosed by mutants with altered phagocytic properties. *J. Cell Biol.* 86:456–465.
60. Watts, C., and M. Marsh. 1992. Endocytosis: what goes in and how? *J. Cell. Sci.* 103:1–8.
61. Wessels, D.J., J. Murray, G. Jung, J.A. Hammer III, and D.R. Soll. 1991. Myosin IB null mutants of *Dictyostelium* exhibit abnormalities in motility. *Cell Motil. Cytoskeleton.* 20:301–315.